Inorg. Chem. **2006**, *45*, 2835–2856

Quantum Chemistry-Based Analysis of the Vibrational Spectra of Five-Coordinate Metalloporphyrins [M(TPP)Cl]

Florian Paulat, V. K. K. Praneeth, Christian Näther, and Nicolai Lehnert*

Institut für Anorganische Chemie, Christian-Albrechts-Universität Kiel, Olshausenstrasse 40, D-24098 Kiel, Germany

Received June 30, 2005

Vibrational properties of the five-coordinate porphyrin complexes [M(TPP)(Cl)] (M = Fe, Mn, Co) are analyzed in detail. For [Fe(TPP)(Cl)] (**1**), a complete vibrational data set is obtained, including nonresonance (NR) Raman, and resonance Raman (RR) spectra at multiple excitation wavelengths as well as IR spectra. These data are completely assigned using density functional (DFT) calculations and polarization measurements. Compared to earlier works, a number of bands are reassigned in this one. These include the important, structure-sensitive band at 390 cm^{-1}, which is reassigned here to the totally symmetric $\nu_{breathing}$(Fe–N) vibration for complex **1**. This is in agreement with the assignments for [Ni(TPP)]. In general, the assignments are on the basis of an idealized $[M(TPP)]^+$ core with D_{4h} symmetry. In this Work, small deviations from D_{4h} are observed in the vibrational spectra and analyzed in detail. On the basis of the assignments of the vibrational spectra of **1**, [Mn(TPP)(Cl)] (**2**), and diamagnetic [Co(TPP)(Cl)] (**3**), eight metal-sensitive bands are identified. Two of them correspond to the ν(M–N) stretching modes with B_{1g} and E_u symmetries and are assigned here for the first time. The shifts of the metal sensitive modes are interpreted on the basis of differences in the porphyrin C–C, C–N, and M–N distances. Besides the porphyrin core vibrations, the M–Cl stretching modes also show strong metal sensitivity. The strength of the M–Cl bond in **1**–**3** is further investigated. From normal coordinate analysis (NCA), force constants of 1.796 (Fe), 0.932 (Mn), and 1.717 (Co) mdyn/Å are obtained for **1**–**3**, respectively. The weakness of the Mn–Cl bond is attributed to the fact that it only corresponds to half a σ bond. Finally, RR spectroscopy is used to gain detailed insight into the nature of the electronically excited states. This relates to the mechanism of resonance enhancement and the actual nature of the enhanced vibrations. It is of importance that anomalous polarized bands (A_{2g} vibrations), which are diagnostic for vibronic mixing, are especially useful for this purpose.

Introduction

Vibrational spectroscopy is a very valuable method that is used to gain insight into the electronic structures of metalloporphyrins. Especially, heme proteins that contain iron porphyrins as prosthetic groups have been studied in detail, and information about the properties of their heme cofactors have been obtained because of the sensitivity of the vibrational frequencies to the changes in oxidation state, coordination number, and spin state.[1,2] Hemes occur as active sites in many different proteins and have been characterized by all types of spectroscopic methods. Among these, resonance Raman (RR) spectroscopy has always played a key role. RR spectroscopy selectively enhances the vibrational modes of the absorbing chromophore, whereas the remaining vibrational modes in the molecule (protein) are suppressed.[3−5] In this way, RR spectra of a heme chromophore can be obtained selectively even in a large molecule (protein) where many other vibrations are present. From the vibrational energies as well as the nature of the enhanced modes, information about the geometric and electronic

* To whom correspondence should be addressed. E-mail: nlehnert@ac.uni-kiel.de.

(1) Spiro, T. G. In *Iron Porphyrins;* Lever, A. B. P., Gray, H. B., Eds.; Addison-Wesley: Reading, MA, 1983; Part 2, pp 89−159.
(2) Spiro, T. G.; Li, X.-Y. In *Resonance Raman Spectra of Heme and Metalloproteins;* Spiro, T. G., Ed.; Wiley: New York, 1988; pp 1−37.
(3) Spiro, T. G.; Czernuszewicz, R. S. In *Physical Methods in Bioinorganic Chemistry;* Que, L., Jr., Ed.; University Science Books: Sausalito, CA, 2000; pp 59−120.
(4) Loehr, T. M. In *Spectroscopic Methods in Bioinorganic Chemistry;* Solomon, E. I., Hodgson, K. O., Eds.; American Chemical Society: Washington, DC, 1998; pp 136−153.
(5) Czernuszewicz, R. S.; Spiro, T. G. In *Inorganic Electronic Structure and Spectroscopy;* Solomon, E. I., Lever, A. B. P., Eds.; John Wiley & Sons: New York, 1999; Vol. 1, pp 353−441.

10.1021/ic0510866 CCC: $33.50
Published on Web 02/28/2006

Scheme 1

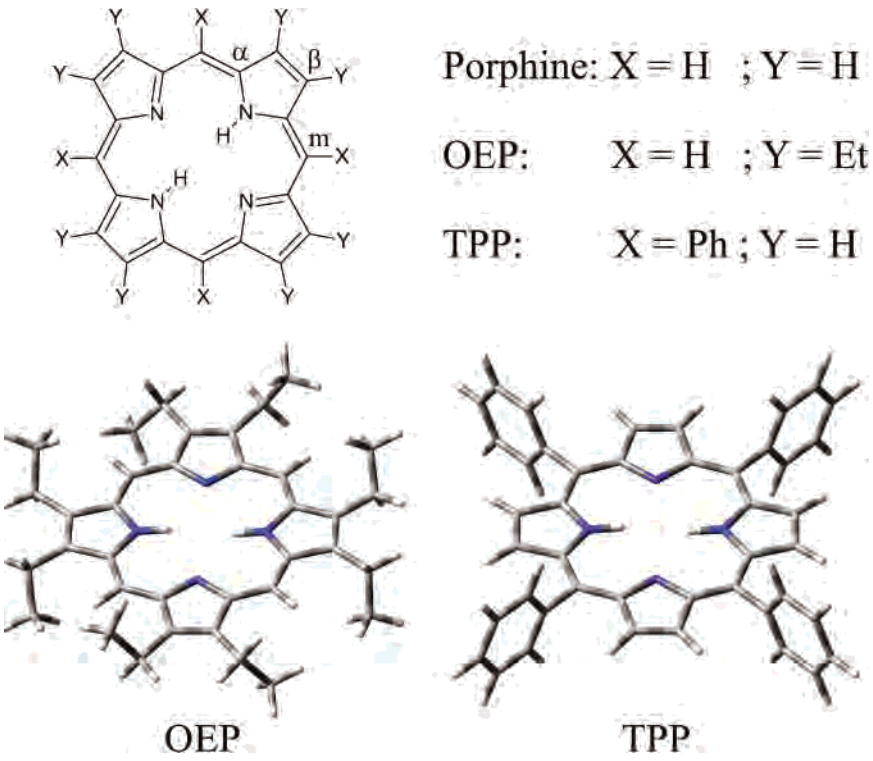

properties of the heme as well as its environment can be obtained.[1,5] Besides the investigation of metalloporphyrins in biological systems, synthetic porphyrin model complexes have been studied widely to gain insight into the catalytic reactions or functions performed by heme proteins.[6] In many cases, tetraphenylporphyrin (TPP) and octaethylporphyrin (OEP) ligands have been used for such model systems. Scheme 1 shows the OEP and TPP ligands, which are based on simple porphine P, where the meso (X) and β substituents (Y) are hydrogen atoms. OEP has ethyl groups in the β position (Y = Et), whereas TPP has phenyl groups in the meso position (X = Ph). The RR spectra of such metalloporphyrin model complexes have been intensely studied, and spectral assignments have been obtained.[1] For the vibrational assignments, four-coordinate Nickel complexes have, in general, been used because they are stable and nonfluorescent. In addition, there are no complications due to axial ligands when using the four-coordinate species. Correspondingly, much effort has been spent to investigate the RR and IR spectra of the Ni(II) complexes [Ni(OEP)] and [Ni(TPP)]. On the basis of multiple isotope substitution, multiple-wavelength RR spectroscopy, and IR measurements, the spectra of [Ni(OEP)] and [Ni(TPP)] have been assigned by different groups. Kitagawa and co-workers assigned most of the infrared and RR in-plane modes of [Ni(OEP)] using variable excitation RR spectra, ^{15}N and C_m-D isotope shifts, and a normal-coordinate analysis (NCA).[7,8] In-plane as well as out-of-plane modes for general metalloporphines [M(P)] were calculated by Warshel and Lappicirella[9] using a semiempirical force field (QCFF/PI). This study provides the first analysis of the out-of-plane vibrations of the porphyrin core. Spiro and co-workers[10] later developed a consistent empirical force field for nickel porphyrins with different substituents, including porphine, OEP, and TPP. The RR spectra of [Ni(TPP)] were completely assigned using pyrrole-$^{15}N_4$, pyrrole-d_8, $^{13}C_4$-meso and phenyl-d_{20} isotopomers, and NCA.[10] Other simple [M(TPP)] complexes (M = Cu(II), Zn(II), and Co(II)) were studied by other groups.[11,12] However, until now, no detailed vibrational assignments of five-coordinate complexes of type [M(P)(X)] existed.

In contrast to the RR spectra, the IR spectra of TPP complexes remained unassigned for a long time because of their complexity. The first complete assignment of an infrared spectrum of a TPP complex was performed by Rush III et al.[13] in 2000 for [Ni(TPP)] using DFT−SQM calculations. RR intensities were also calculated using the semiempirical INDO method, which led to the reassignment of several RR bands. Hence, these new assignments are on the basis of quantum chemical calculations, which only became available

(6) Walker, F. A. In *Encyclopedia of Inorganic Chemistry;* King, R. B., Ed.; John Wiley & Sons: New York, 1994; Vol. 4, pp 1785−1846.
(7) Kitagawa, T.; Abe, M.; Ogoshi, H. *J. Chem. Phys.* **1978**, *69*, 4516−4525.
(8) Abe, M.; Kitagawa, T.; Kyogoku, Y. *J. Chem. Phys.* **1978**, *69*, 4526−4534.
(9) Warshel, A.; Lappicirella, A. *J. Am. Chem. Soc.* **1981**, *103*, 4664−4673.
(10) Li, X.-Y.; Czernuszewicz, R. S.; Kincaid, J. R.; Su, Y. O.; Spiro, T. G. *J. Phys. Chem.* **1990**, *94*, 31−47. (b) Li, X.-Y.; Czernuszewicz, R. S.; Kincaid, J. R.; Stein, P.; Spiro, T. G. *J. Phys. Chem.* **1990**, *94*, 47−61. (c) Li, X.-Y.; Czernuszewicz, R. S.; Kincaid, J. R.; Spiro, T. G. *J. Am. Chem. Soc.* **1989**, *111*, 7012−7023.
(11) Atamian, M.; Donohoe, R. J.; Lindsey, J. S.; Bocian, D. F. *J. Phys. Chem.* **1989**, *93*, 2236−2243.
(12) Kozuka, M.; Iwaizumi M. *Bull. Chem. Soc. Jpn.* **1983**, *56*, 3165−3166.
(13) Rush, T. S., III; Kozlowski, P. M.; Piffat, C. A.; Kumble, R.; Zgierski, M. Z.; Spiro, T. G. *J. Phys. Chem. B* **2000**, *104*, 5020−5034.

recently for the routine treatment of large molecules such as [Ni(TPP)]. These theoretical methods provide a new tool to researchers that enables them to analyze the missing puzzle pieces of the vibrational assignments of porphyrin complexes, as will be further demonstrated in this study.

Besides the detailed assignments of nickel porphyrin complexes including [Ni(TPP)],[10,14,15] the Spiro group has also analyzed the effects of oxidation- and spin-state changes on the RR spectra of heme proteins.[15b,d−f,42,44] It was concluded that the oxidation-state sensitivity largely depends on the back-bonding between the metal and the porphyrin ring. In the case of iron, back-bonding is greatly reduced for Fe(III) compared to Fe(II) because of a lowering in energy of the d orbitals, which induces shifts in certain porphyrin vibrations. In agreement with this analysis, axial ligands of increasing π-acceptor strength increase the frequencies of the oxidation-state sensitive bands[15e] by competing with the porphyrin ring for the iron d_π electrons. Correspondingly, using the strong π donor ligand cysteine, these oxidation-state sensitive bands shift to energies below the typical range associated with nonacceptor ligands.[16] Spin-sensitivity, on the other hand, has been attributed to ring conformation.[15b] Doming of the porphyrin ring occurs as a consequence of out-of-plane displacement of iron,[15b] which is due to the fact that high-spin iron(II) and iron(III) are too large to fit into the center of the porphyrin ring. In this way, the high-spin state of iron causes doming that then induces band shifts. On the other hand, Spaulding et al.[17] suggested that the core size is the dominant parameter for spin-state sensitivity. Because of the out-of-plane displacement of the iron atom, the pyrrole rings are expected to tilt to maintain the overlap with the metal orbitals. This leads to a lowering of certain vibrational frequencies because of the loss of π conjugation at the methine bridges of the porphyrin ring. Hence, both core expansion and pyrrole tilting are expected to contribute to the lowering of vibrational frequencies, where core expansion is dominant at moderate tilt angles.[15f] Altogether, five structure sensitive RR signals were described in the literature and designated as bands A−E. These oxidation- and spin-state sensitive bands are also expected to be sensitive to the nature of the metal ion because of the variable occupation and energies of the d orbitals of different metals.[18] Oshio et al.[18b] observed metal-sensitivity in the IR spectra of [M(TPP)] complexes. The frequencies of these bands I−III were found to decrease as the metal−porphyrinato nitrogen distances increased (Ni(II) > Co(II) > Cu(II) > Zn(II)).

In this study, density functional theory (DFT) is used to calculate the IR and Raman spectra of the five-coordinate complexes [M(TPP)(Cl)] with M = Fe (**1**), Mn (**2**), and Co (**3**). On the basis of these results, the experimental nonresonance Raman (NR Raman), resonance Raman, and IR spectra of compound **1** are assigned in detail for the first time. The calculated Raman spectra cannot be compared to resonance Raman measurements because of the difference in the selection rules for resonance and nonresonance Raman scattering.[19] Therefore, using an excitation wavelength of 1064 nm, the nonresonance Raman spectra of **1**, including polarized measurements are presented for the first time. Resonance Raman spectra at multiple excitation wavelengths have also been obtained for **1**, which, together with polarized measurements, allow for the assignments of additional bands. Altogether, a complete assignment of all available experimental data has been achieved for compound **1**. These results are then compared to an earlier assignment[20] of a few RR bands of **1** in the 1000−1600 cm^{-1} range. Results of Burke et al.,[14] who roughly classified the vibrations of compound **1** on the basis of RR isotope shifts and polarization measurements, are also taken into consideration. The vibrational assignments obtained for **1** are then compared to the assignments of the Raman and IR spectra of **2** and **3** to identify the metal-sensitive bands. Not surprisingly, one of the most metal-sensitive bands in these complexes is the metal−chloride stretching vibration. These are identified in the IR spectra of **1**−**3**, and the corresponding force constants are determined using the quantum-chemistry centered normal coordinate analysis (QCC−NCA).[21] Finally, the correlation of our results to the detailed assignments for [Ni(TPP)] is also included.[13] Going from [Ni(TPP)] to [M(TPP)(Cl)] type complexes adds the complexity of having (a) open shells, (b) larger distortions of the porphyrin ring, and (c) axial ligands. The influence of these electronic and structural differences on the vibrational spectra of metalloporphyrins is analyzed.

Experimental and Computational Procedures

Syntheses. The complexes [Fe(TPP)(Cl)] (**1**) and [Mn(TPP)(Cl)] (**2**) were synthesized using published procedures[22] and isolated as microcrystalline solids. Complex [Co(TPP)Cl] (**3**) was synthesized using the procedure by Mahmood et al.[23] Single Crystals of **2** were obtained by slow diffusion of *n*-hexane into a solution of **2** in

(14) Burke, J. M.; Kincaid, J. R.; Spiro, T. G. *J. Am. Chem. Soc.* **1978**, *100*, 6077−6083. (b) Burke, J. M.; Kincaid, J. R.; Peters, S.; Gagne, R. R.; Collman, J. P.; Spiro, T. G. *J. Am. Chem. Soc.* **1978**, *100*, 6083−6088.

(15) Spiro, T. G. In *Iron Porphyrins*; Lever, A. B. P., Gray, H. B., Eds.; Addison-Wesley: Reading, MA, 1983; Part 2, pp 89−159. (b) Spiro, T. G.; Strekas, T. C. *J. Am. Chem. Soc.* **1974**, *96*, 338−345. (c) Spiro, T. G.; Strekas, T. C. *Proc. Natl. Acad. Sci. U.S.A.* **1972**, *69*, 2622−2626. (d) Burke, J. M.; Kincaid, J. R.; Peters, S.; Gagne, R. R.; Collman, J. P.; Spiro, T. G. *J. Am. Chem. Soc.* **1978**, *100*, 6083−6088. (e) Spiro, T. G.; Burke, J. M. *J. Am. Chem. Soc.* **1976**, *98*, 5482−5489. (f) Spiro, T. G.; Stong, J. D.; Stein, P. *J. Am. Chem. Soc.* **1979**, *101*, 2648−2655.

(16) Champion, P. M.; Gunsalus, I. C. *J. Am. Chem. Soc.* **1977**, *99*, 2000−2002. (b) Champion, P. M.; Gunsalus, I. C.; Wagner, G. C. *J. Am. Chem. Soc.* **1978**, *100*, 3743−3751.

(17) Spaulding, L. D.; Chang, C. C.; Yu, N.-T.; Felton, R. H. *J. Am. Chem. Soc.* **1975**, *97*, 2517−2525.

(18) Kincaid, J.; Nakamoto, K. *J. Inorg. Nucl. Chem.* **1975**, *37*, 85. (b) Oshio, H.; Ama, T.; Watanabe, T.; Kincaid, J.; Nakamoto, K. *Spectrochim. Acta, Part A* **1984**, *40*, 863−870.

(19) Tang, J.; Albrecht, A. C. In *Raman Spectroscopy;* Szymanski, H. A., Ed.; Plenum Press: New York, 1970; Vol. 2. (b) Albrecht, A. C. *J. Chem. Phys.* **1961**, *34*, 1476.

(20) Czernuszewicz, R. S.; Macor, K. A.; Li, X.-Y.; Kincaid, J. R.; Spiro, T. G. *J. Am. Chem. Soc.* **1989**, *111*, 3860−3869.

(21) Lehnert, N.; Tuczek, F. *Inorg. Chem.* **1999**, *38*, 1659−1670. (b) Praneeth, V. K. K.; Näther, C.; Peters, G.; Lehnert, N. *Inorg. Chem.*, in press.

(22) Adler, A. D.; Longo, F. R.; Kampas, F.; Kim, J. *J. Inorg. Nucl. Chem.* **1970**, *32*, 2443−2445.

(23) Mahmood, A.; Liu, H.-I.; Jones, J. G.; Edwards, J. O.; Sweigart, D. A. *Inorg. Chem.* **1988**, *27*, 2149−2154.

$CHCl_3$. The identity of the compounds was established using ^1H NMR and UV−vis absorption spectroscopy and mass spectrometry (for compound **2**).

Crystal Structure Determination. The data were collected using an STOE imaging plate diffraction system (IPDS). The structure was solved with direct methods using SHELXS-97 and was refined against F^2 using SHELXL-97. All non-H atoms were refined anisotropically, except for some of the chlorine atoms of the disordered chloroform molecule. The H atoms were positioned with idealized geometry and refined using a riding model. The chloroform molecule is disordered and was refined using a split model.

Vibrational Spectroscopy. FT-Raman spectra were recorded on a Bruker IFS 66 interferometer with a Bruker FRA 106 Raman attachment using an Nd:YAG laser for excitation ($\lambda = 1064$ nm). Measurements were performed on pure compounds. The polarized FT-Raman spectra of **1** were measured in CH_2Cl_2. Resolution was set to 2 cm^{-1}. Resonance Raman spectra were measured on a Dilor XY Raman spectrograph with a triple monochromator and a CCD detector. An Ar/Kr mixed-gas laser with a maximum power of 5 W was used for excitation. The spectra were measured on KBr disks cooled to 10 K with a helium cryostat. The spectral band pass was set to 2 cm^{-1}. Middle- and far-infrared spectra (MIR and FIR) were recorded on a Bruker IFS 66v vacuum instrument at room temperature. For the MIR region, KBr disks were used, and the spectra were recorded at a resolution of 1 cm^{-1}. FIR spectra were obtained on PE pellets at a resolution of 2 cm^{-1}.

UV−Vis Spectroscopy. Absorption spectra were recorded in chloroform for **1**, in a 1/1 mixture of butyronitrile and propionitrile for **2**, and in methanol solution for **3** at room temperature using a Varian Cary 5 UV−vis NIR spectrometer. The absorption data were scaled using literature extinction coefficients as indicated in Figure 7.

Density Functional Calculations. DFT calculations using Becke's three parameter hybrid functional with the correlation functional of Lee, Yang, and Parr (B3LYP[24]) were performed using the program package Gaussian 03.[25] The structures of the compounds [Fe(TPP)(Cl)] ($S = {}^5/_2$), [Mn(TPP)(Cl)] ($S = 2$), and [Co(TPP)(Cl)] ($S = 0$) were fully optimized without simplifications using the LanL2DZ basis set. Calculated vibrational frequencies for **1** show that the obtained geometry represents a true minimum because no imaginary frequency is obtained. For compounds **2** and **3**, one imaginary frequency ($<6i$ cm^{-1}) is calculated, which corresponds to the out-of-plane deformation mode of the ruffling type[26] (B_{1u}) at low energy. Infrared and Raman intensities were calculated as well. In all calculations, convergence was reached when the relative change in the density matrix between subsequent iterations was less than 1×10^{-8}. The structures of the models [Fe(P)(Cl)] (P = porphine; $\tilde{\mathbf{1}}$, $S = {}^5/_2$), [Mn(P)(Cl)] ($\tilde{\mathbf{2}}$, $S = 2$), and [Co(P)(Cl] ($\tilde{\mathbf{3}}$, $S = 0$) have also been fully optimized using B3LYP/LanL2DZ. For these calculations, the TPP ligand has been simplified to porphine (Scheme 1). The illustrations of the local coordinates of bromobenzene (cf. Figure 3) were obtained using the program GaussView.

Normal Coordinate Analysis (NCA). Normal coordinate calculations were performed using the QCPE computer program 576 by M. R. Peterson and D. F. McIntosh. The calculations are on the basis of a general valence force field and the force constants are refined with a nonlinear simplex algorithm. The simplex optimization was used to refine only selected force constants according to the quantum-chemistry centered normal coordinate analysis (QCC−NCA) scheme.[21] Here, a force field from DFT calculations is used as a starting point to generate initial force constants, and a subset of these is fitted to reproduce the known experimental frequencies. Force constants were obtained from the Gaussian output using a modified version of the program Redong[27] (QCPE 628). For the normal coordinate analysis, model complexes $\tilde{\mathbf{1}}-\tilde{\mathbf{3}}$ were modified by using a mass of 77 corresponding to a phenyl group for the hydrogens of the meso carbon atoms. This leads to models [Fe(P*)Cl] ($\tilde{\mathbf{1}}$**a**), [Mn(P*)Cl] ($\tilde{\mathbf{2}}$**a**), and [Co(P*)Cl] ($\tilde{\mathbf{3}}$**a**).

Results and Analysis

A. Crystal and DFT-optimized Structures of [Fe(TPP)(Cl)] (1), [Mn(TPP)(Cl)] (2), and [Co(TPP)Cl] (3). To calculate the vibrational spectra of **1**−**3**, their geometric structures have to be fully optimized first. In this section, the calculated structures are compared to the experimental ones, and in addition, a new crystal structure of the chloroform solvate of complex **2** is presented. Altogether, satisfactory agreement between the DFT calculations and experiment is obtained. Considering the porphyrin core bond lengths, excellent agreement with experiment is achieved in this study, as shown in Table S6.

A.1. Crystal and DFT Structures of Compound 1. The crystal structure of the tetragonal form of compound **1** has been determined by Hoard et al.[28] Later, Scheidt and Finnegan[29] obtained the structure of a monoclinic form of this complex. The monoclinic form differs significantly from the tetragonal form. It shows a small C_{4v} doming and a displacement of the iron from the N_4 plane by $\Delta Fe-Ct = 0.49$ Å. In contrast, the tetragonal form has an almost planar porphyrin core. Because of the conditions applied to the preparation of the compound (solvent used for recrystallization), it can be assumed that our compound corresponded to the tetragonal form. In this structure, the axial Fe−Cl bond is 2.192 Å, the averaged Fe−N distance is 2.049 Å, and the out-of-plane displacement of the iron atom is $\Delta Fe-Ct = 0.383$ Å. Figure 1A shows the DFT-optimized structure of **1**, which shows an overall good agreement with the crystal structure. In both cases, the porphyrin ring is almost planar

(24) Becke, A. D. *Phys. Rev. A: At., Mol., Opt. Phys.* **1988**, *38*, 3098. (b) Becke, A. D. *J. Chem. Phys.* **1993**, *98*, 1372. (c) Becke, A. D. *J. Chem. Phys.* **1993**, *98*, 5648.

(25) Frisch, M. J.; Trucks, G. W.; Schlegel, H. B.; Scuseria, G. E.; Robb, M. A.; Cheeseman, J. R.; Montgomery, J. A., Jr.; Vreven, T.; Kudin, K. N.; Burant, J. C.; Millam, J. M.; Iyengar, S. S.; Tomasi, J.; Barone, V.; Mennucci, B.; Cossi, M.; Scalmani, G.; Rega, N.; Petersson, G. A.; Nakatsuji, H.; Hada, M.; Ehara, M.; Toyota, K.; Fukuda, R.; Hasegawa, J.; Ishida, M.; Nakajima, T.; Honda, Y.; Kitao, O.; Nakai, H.; Klene, M.; Li, X.; Knox, J. E.; Hratchian, H. P.; Cross, J. B.; Bakken, V.; Adamo, C.; Jaramillo, J.; Gomperts, R.; Stratmann, R. E.; Yazyev, O.; Austin, A. J.; Cammi, R.; Pomelli, C.; Ochterski, J. W.; Ayala, P. Y.; Morokuma, K.; Voth, G. A.; Salvador, P.; Dannenberg, J. J.; Zakrzewski, V. G.; Dapprich, S.; Daniels, A. D.; Strain, M. C.; Farkas, O.; Malick, D. K.; Rabuck, A. D.; Raghavachari, K.; Foresman, J. B.; Ortiz, J. V.; Cui, Q.; Baboul, A. G.; Clifford, S.; Cioslowski, J.; Stefanov, B. B.; Liu, G.; Liashenko, A.; Piskorz, P.; Komaromi, I.; Martin, R. L.; Fox, D. J.; Keith, T.; Al-Laham, M. A.; Peng, C. Y.; Nanayakkara, A.; Challacombe, M.; Gill, P. M. W.; Johnson, B.; Chen, W.; Wong, M. W.; Gonzalez, C.; Pople, J. A. *Gaussian 03*, revision C.02; Gaussian, Inc.: Wallingford, CT, 2004.

(26) Jentzen, W.; Song, X.-Z.; Shelnutt, A. *J. Phys. Chem. B* **1997**, *101*, 1684−1699.

(27) Allouche, A.; Pourcin, J. *Spectrochim. Acta, Part A* **1993**, *49*, 571.

(28) Hoard, J. L.; Cohen, G. H.; Glick, M. D. *J. Am. Chem. Soc.* **1967**, *89*, 1992−1996.

(29) Scheidt, W. R.; Finnegan, M. G. *Acta Crystallogr., Sect. C* **1989**, *45*, 1214−1216.

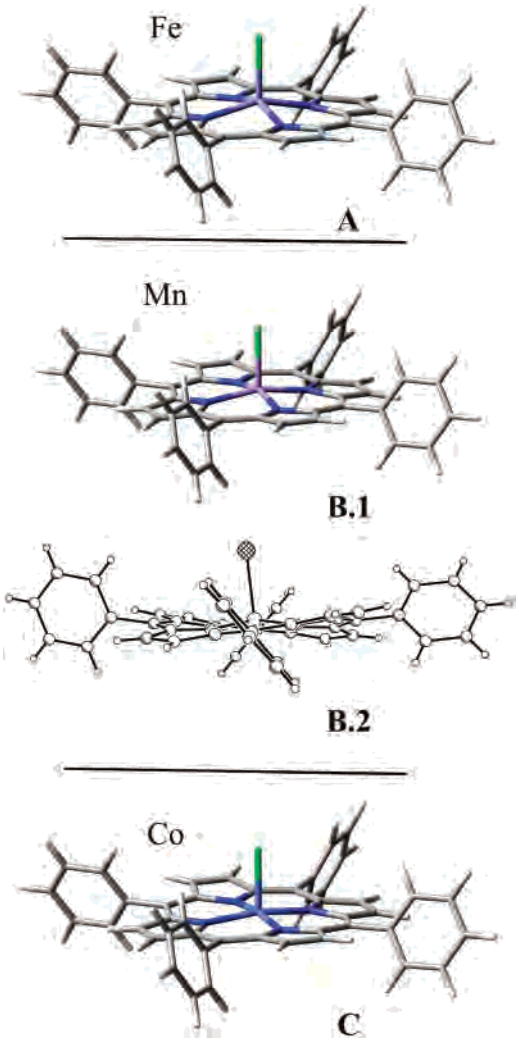

Figure 1. DFT optimized structure of **1** (A); DFT optimized structure of **2** (B.1); the crystal structure of **2** in side view (B.2); and DFT optimized structure of **3** (C).

and the phenyl rings are slightly tilted. The DFT structure also shows a very small amount of saddling of the porphyrin ring, which is not observed experimentally. The calculated Fe−N distance of 2.09 Å and the obtained Fe−Ct distance of 0.45 Å are in very good agreement with experiment. Therefore, a good theoretical description of the $[Fe(TPP)]^+$ core of **1** has been obtained. The largest deviation in the calculated structure is observed for the Fe−Cl bond distance of 2.32 Å, which is too long.

A.2. Crystal and DFT Structures of Compound 2. In the new crystal structure presented here, compound **2** crystallizes in the monoclinic space group $P2_1/n$ with four formula units in the unit cell and all atoms located in general positions. The porphyrin moiety is saddled and shows a deviation of the atoms from the best least-squares plane of about 0.29 Å. The manganese atom is located 0.258 Å above the plane formed by the four nitrogen atoms. The averaged manganese nitrogen distance is 2.019 Å, and hence it is between the values for **1** and **3** (vide infra). The obtained manganese chloride distance is 2.389 Å. Note that the crystal structures of **2** as toluene[30] or acetone[31] solvate are very similar. Larger deviations are observed for the solvate's free

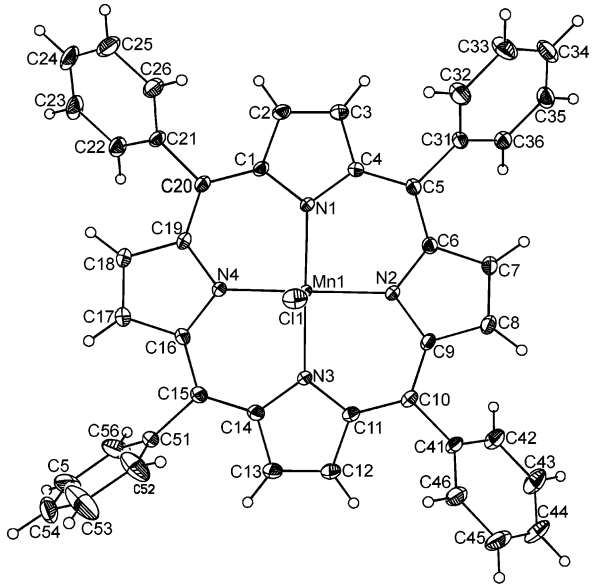

Figure 2. Crystal structure of compound **2** with labeling. Displacement ellipsoids are drawn at the 50% probability level.

crystal structure,[32] which shows an almost planar porphyrin core. The DFT-optimized and the crystal structures of **2** (chloroform solvate) are shown in Figures 1B and 2. In contrast to the crystal structure, the optimized structure shows an almost planar porphyrin core with a small amount of saddling present. The averaged manganese nitrogen distance of 2.036 Å and the Mn−Cl distance of 2.420 Å, however, are both in very good agreement with experiment. In addition, the calculated displacement of the manganese atom from the nitrogen N_4 plane of the porphyrin is 0.28 Å and hence, close to the experimental value. Therefore, in this case, the largest deviation of the calculated structure is observed for the ring conformation of the TPP ligand.

A.3. Crystal and DFT Structures of Compound 3. The crystal structure of [Co(TPP)(Cl)] shows a body-centered tetragonal unit cell.[33] The coordination geometry of the Co(III) ion corresponds to a pyramid, where the cobalt atom is displaced from the porphyrin plane by only 0.05 Å. The porphyrin ring itself is almost planar. Bond distances of 1.985 Å for Co−N and 2.145 Å for Co−Cl are observed. The DFT-optimized structure of **2** is shown in Figure 1C. The optimized structure shows an almost planar porphyrin core in agreement with experiment, with a small amount of saddling present. The calculated Co−N distance of 1.99 Å is in excellent agreement with the crystal structure, whereas the out-of-plane displacement of ΔCo−Ct = 0.17 Å is somewhat overestimated. As in the case of **1**, the largest deviation is observed for the Co−Cl distance, which is calculated to be 2.25 Å.

B. Vibrational Spectra and Assignment of Compound 1. As mentioned in the Introduction, earlier vibrational

(30) Armstrong, R. S.; Foran, G. J.; Hambley, T. W. *Acta Crystallogr., Sect. C* **1993**, *49*, 236−238.
(31) Tulinsky, A.; Chen, B. M. L. *J. Am. Chem. Soc.* **1977**, *99*, 3647−3651.
(32) Cheng, B.; Scheidt, W. R. *Acta Crystallogr., Sect. C* **1996**, *52*, 361−363.
(33) Sakurai, T.; Yamamoto, K.; Naito, H.; Nakamoto, N. *Bull. Chem. Soc. Jpn.* **1976**, *49*, 3042−3046.

analyses of [Fe(TPP)(Cl)] were restricted to the RR spectrum obtained for the Soret excitation.[20] Additionally, three IR bands of **1** were assigned, which are considered to be structure-sensitive.[18b] Here, we report the nonresonance Raman (NR Raman) spectrum of **1**, including polarized measurements for the first time. Complete assignments of these data are achieved using DFT calculations. In addition, RR data measured at variable wavelengths including new polarized data are presented and used to assign additional bands. Finally, the IR spectrum of **1** is assigned.

B.1. Classification of the TPP Vibrations Using Group Theory. To assign the vibrational spectra of **1**, an effective D_{4h} symmetry was applied. The analysis of the polarized data (cf. section B.5) shows that this approach is justified even for five-coordinate compounds such as **1**−**3**. D_{4h} symmetry is obtained for a planar porphyrin core with the metal being located in the plane with no axial ligand present. The phenyl rings are exactly perpendicular to the porphyrin plane. In this D_{4h} model system [M(TPP)] (idealized metalloporphyrin), the planar porphyrin core has 71 in-plane modes:[10a]

$$\Gamma_{\text{in plane}} = 9A_{1g}(R) + 8A_{2g}(RR) + 9B_{1g}(R) + 9B_{2g}(R) + 18E_u(IR) \quad (1)$$

In the NR Raman spectrum, 27 in-plane vibrations are therefore expected, 9 of them polarized (A_{1g}) and 18 of them depolarized (B_{1g} and B_{2g}). The infrared spectrum shows a maximum of 18 modes with E_u symmetry. In addition, the porphyrin core of the D_{4h} model system has 34 out-of-plane vibrations:[10a]

$$\Gamma_{\text{out of plane}} = 3A_{1u} + 6A_{2u}(IR) + 4B_{2u} + 5B_{1u} + 8E_g(R) \quad (2)$$

The eight E_g modes are Raman-active, and the six A_{2u} modes are infrared-active. Therefore, on the basis of a purely statistical consideration, many more in-plane than out-of-plane modes can be expected in the NR Raman and IR spectra of metalloporphyrins. To classify the different porphyrin core vibrations, the local coordinates defined by Li et al.[10] are used (cf. Figures S6 and S7) in the following analysis of these spectra.

Besides the porphyrin core modes, a large number of phenyl vibrations are also present in TPP complexes. Different approaches can be taken in the classification of these vibrations. For example, Stein et al.[34] identified several phenyl modes in [(FeTPP)$_2$O] using biphenyl as the model system.[35] To give an intuitive assignment of the phenyl modes of TPP, we use bromobenzene as the model. Table 2 provides a complete list of all normal modes of bromobenzene together with calculated energies and assignments using local coordinates. Figure 3 shows the important phenyl vibrations in bromobenzene that are also observed in the spectra of **1**−**3**. The TPP ligand itself has four phenyl groups that are bound to the meso carbon atoms of the porphyrin core. Hence, for every local phenyl coordinate, there are four symmetry-adapted combinations in TPP. Because the interactions of the local vibrations of different phenyl rings are small, the obtained splittings between the resulting four combinations are also small (usually 5−10 cm^{-1}). Hence, the four resulting symmetry-adapted linear combinations are also designated as a symmetry block because they are close in energy. Because there are four different irreducible representations in C_{2v} (the point group of bromobenzene), four different symmetry blocks exist:

$$\text{out-of-plane: } B_1 \rightarrow B_{1g}(R) + A_{2g}(RR) + E_u(IR) \quad (\pi, \pi', \text{and } \pi'') \quad (3)$$

$$\text{out-of-plane: } A_2 \rightarrow A_{1u} + B_{2u} + E_g(R) \quad (\sigma, \sigma', \text{and } \sigma'') \quad (4)$$

$$\text{in-plane: } B_2 \rightarrow B_{1u} + A_{2u}(IR) + E_g(R) \quad (\psi, \psi', \text{and } \psi'') \quad (5)$$

$$\text{in-plane: } A_1 \rightarrow A_{1g}(R) + B_{2g}(R) + E_u(IR) \quad (\phi, \phi', \text{and } \phi'') \quad (6)$$

The nomenclature (π, σ, ψ, and ϕ) is taken from ref 10. To classify the different porphyrin core and phenyl modes in D_{4h} symmetry, we used the idealized model [Zn(TPP)] and calculated the vibrations of this model in D_{4h} symmetry. [Zn(TPP)] has 169 normal modes (56 of them are degenerate), where 44% are Raman- and 27% are IR-active.

B.2. NR Raman Spectrum and Assignment of 1. The experimental and calculated NR Raman spectra of **1** are shown in the top panel of Figure 4. Corresponding polarized data are included in the lower panel. The calculated spectrum is, in general, shifted to a somewhat higher energy (the average deviation in vibrational energies is about 2 to 3%) compared to experiment, which is further evaluated in the discussion. Besides the good agreement in vibrational frequencies, very good agreement with experiment is obtained for the calculated NR Raman intensities, as shown in Figure 4 (top). This allows for a detailed assignment of the data. Importantly, additional information to support the Raman assignments is available from polarization measurements. The depolarization ratio ρ is defined as $\rho = I_{\text{perpendicular}}/I_{\text{parallel}}$. In D_{4h} symmetry, one obtains[1]

Table 1. Crystal Data and Results of Structure Refinement for Compound **2**

cmpd	**2**
chemical formula	$C_{44}H_{28}N_4MnCl \cdot CHCl_3$
fw	822.46
$T =$	150 K
$\lambda =$	0.71073
crystal system	monoclinic
space group	$P2_1/n$
$a =$	12.157 (1) Å
$b =$	21.899 (2) Å
$c =$	14.479 (1) Å
$\beta =$	102.05 (1)
$V =$	3769.7 (4) Å^3
Z	4
$D_{\text{calcd}} =$	1.449 g·cm^{-3}
$\mu =$	0.67 mm^{-1}
R1[a] [$I > 2\sigma(I)$]	0.0392
wR2[b] [all data]	0.1053

[a] $R1 = \Sigma ||Fo| - |Fc||/\Sigma|Fo|$. [b] $wR2 = [\Sigma[w(F_o^2 - F_c^2)^2]/\Sigma[w(F_o^2)^2]]^{1/2}$.

(34) Stein, P.; Ulman, A.; Spiro, T. G. *J. Phys. Chem.* **1984**, *88*, 369−374.
(35) Zerbi, G.; Sandioni, S. *Spectrochim. Acta, Part A* **1968**, *24*, 511.

Table 2. Calculated Vibrational Energies (cm^{-1}) of Bromobenzene and Assignments Using Local Coordinates

	frequencies				frequencies		
$\nu(Ph)_i$	calcd[a]	assignment[b]	sym.[c]	$\nu(Ph)_i$	calcd[a]	assignment[b]	sym.[c]
1	167	γ(Br)	B_1	16	1082	ν_1(C−C)	A_1
2	242	δ(C−C−Br)	B_2	17	1098	ν_{asym1}(C−C) + δ(C−C−H)	B_2
3	301	ν(C−Br)	A_1	18	1206	δ_{asym}(C−C−H)	B_2
4	419	τ(ringtwist)	A_2	19	1216	δ_{sym}(C−C−H)	A_1
5	475	γ_1(C)	B_1	20	1344	δ(C−C−H) + ν_2(C−C)	B_2
6	627	δ_1(C−C−C)	B_2	21	1364	ν_{asym2}(C−C)	B_2
7	669	δ_2(C−C−C)	A_1	22	1468	ν_{asym3}(C−C) + δ(C−C−H)	B_2
8	712	γ_2(C)	B_1	23	1499	δ(C−C−H) + ν_{asym4}(C−C)	A_1
9	773	γ_1(H)	B_1	24	1621	ν_{sym}(C−C)	A_1
10	870	γ_2(H)	A_2	25	1629	ν_3(C−C)	B_2
11	952	γ_3(H)	B_1	26	3198	ν(C−H)	A_1
12	1009	δ_{sym}(C−C−C)	A_1	27	3209	ν(C−H)	B_2
13	1014	τ_1	A_2	28	3224	ν(C−H)	A_1
14	1032	$\nu_{breathing}$(C−C)	A_1	29	3235	ν(C−H)	B_2
15	1038	τ_2	B_1	30	3242	ν(C−H)	A_1

[a] Calculated with B3LYP/LanL2DZ; see the Experimental section. [b] Assignments using local coordinates; see Figure 3. [c] Symmetries in the point group C_{2v}.

(1) $0 < \rho < 0.75$ for polarized bands (A_{1g} vibrations),

(2) $\rho = 0.75$ for depolarized bands (B_{1g} or B_{2g} vibrations), and

(3) $\rho > 0.75$ for anomalous polarized bands (A_{2g} vibrations (only RR spectroscopy)).

Hence, *the polarized measurements allow for the determination of the symmetry of a particular mode.*[36] The complete assignments obtained in this manner are listed in Table 3. Additionally, the d_8 isotope shifts available for a number of bands from the RR measurements[14b] are used for comparison with calculated isotope shifts to further confirm our assignments. For a better comparison with the literature, the notation established by Spiro and co-workers for [Ni(TPP)] is used in Table 3. Correspondingly, the porphyrin in-plane modes (both stretching and deformation modes) are labeled ν_i and the porphyrin out-of-plane modes are designated as γ_i.[13] The phenyl mode notation is on the basis of the different symmetry blocks (eqs 3−6). For the oxidation- and spin-state sensitive modes, the common notation from the literature is included in Table 3, where bands A(p), B(dp), C(ap), D(p), and E(p)[18b] are observed in the RR spectra and bands I, II, and III are found in the IR spectra.[18b,42]

The NR Raman spectrum of **1** in Figure 4 can be divided into four regions showing different kinds of vibrations. In the low-energy region between 200 and 500 cm^{-1}, two phenyl out-of-plane vibrations, one porphyrin out-of-plane deformation, and three in-plane porphyrin vibrations are observed (cf. Table 3). The mode at 199 cm^{-1} (calcd: 202 cm^{-1}) corresponds to the Fe−N stetching vibration of B_{1g} symmetry (ν_{18}) and is therefore depolarized. The mode at 390 cm^{-1} (calcd: 388 cm^{-1}) is known to be oxidation-state-sensitive (band E(p)[18b]) and was assigned previously to a porphyrin core deformation mode.[14,18b] However, on the basis of the calculations and the fact that this mode shows strong Soret resonance enhancement, it is assigned to the totally symmetric $\nu_{breathing}$(Fe−N) vibration (ν_8). This is in agreement with the assignments for [Ni(TPP)].[10a,13] The calculated d_8 isotope shift for this mode of 8 cm^{-1} is in very good agreement with the experimental value of 10 cm^{-1}.[14b] The weak band at 379 cm^{-1} (calcd: 336 cm^{-1}) corresponds to the Fe−Cl stretching vibration, which is strongly IR-active (vide infra). The very weak band at 257 cm^{-1} (calcd: 251 cm^{-1}) belongs to the Raman-forbidden γ(Pyr. tilting) vibration of B_{2u} symmetry, which gains intensity through coupling with the Raman allowed γ(Phenylrot.) phenyl vibration of B_{1g} symmetry. Hence, the fact that this mode appears in the Raman spectra is a true effect of the symmetry lowering in **1**. Correspondingly, the very weak feature at 247 cm^{-1} (calcd: 241 cm^{-1}) is assigned to the γ(Phenylrot.) phenyl vibration with B_{1g} symmetry, which is mixed with the γ(Pyr. tilting) porphyrin core vibration with A_{2u} symmetry.

In the energy range from 800 to 1050 cm^{-1}, two weak bands are observed that are assigned to porphyrin core modes. The feature at 994 cm^{-1} (calcd: 1008 cm^{-1}) corresponds to ν(Pyr. breathing) with phenyl contribution (ν_6; cf. Table 3), and the band at 886 cm^{-1} (calcd: 898 cm^{-1}) corresponds to a totally symmetric in-plane deformation mode. This latter vibration was originally assigned to a phenyl vibration,[14] which, based on our calculations is described as a mixed δ_{sym}(Pyr. deformation) and phenyl mode (ν_7). The calculated d_8 isotope shift is 5 cm^{-1}, which is in

(36) Depolarization ratios for some of the weaker bands are difficult to determine from the polarized NR Raman spectrum in Figure 4. In these cases, the depolarization ratios from RR measurements were used. For example, the band at 1364 cm^{-1} is strongly enhanced in Soret resonance, where the depolarized band at 1371 cm^{-1} is not observed. Hence, from the Soret resonance spectrum, the depolarization ratio of this band can be determined.

(37) For the two weak bands at 1275 and 1467 cm^{-1}, depolarization ratios that are slightly larger than 0.75 have been obtained. However, these bands are enhanced in Q and Q_v resonance and are depolarized in these spectra. In addition, anomalous polarized bands (A_{2g}), where $\rho > 0.75$, are forbidden in NR Raman. Hence, the bands at 1275 and 1467 cm^{-1} are classified as dp.

(38) Gouterman, M. In *The Porphyrins*; Dolphin, D., Ed.; Academic Press: New York, 1979; Vol. 3, Part A, pp 1−156.

(39) According to group theory, A_{1g} vibrations could also induce vibronic mixing. However, A_{1g} modes are ineffective because they do not induce a distortion of the molecule.

(40) Czernuszewicz, R. S.; Spiro, T. G. In *Inorganic Electronic Structure and Spectroscopy;* Solomon, E. I., Lever, A. B. P., Eds.; John Wiley & Sons: New York, 1999; Vol. 1, pp 353−441.

(41) Egawa, T.; Suzuki, N.; Dokoh, T.; Higuchi, T.; Shimada, H.; Kitagawa, T.; Ishimura, Y. *J. Phys. Chem. A* **2004**, *108*, 568−577.

(42) Spiro, T. G. *Curr. Sci.* **1998**, *74*, 304−307.

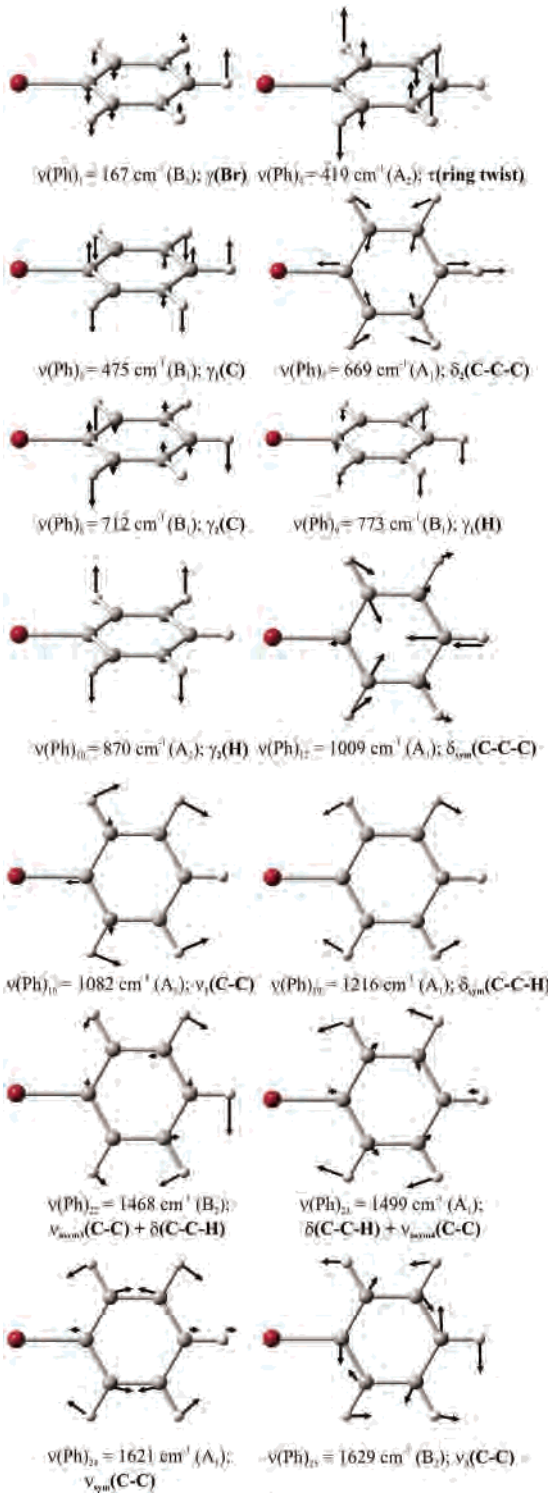

Figure 3. Illustration of the local coordinates of bromobenzene used for classification of in-plane and out-of plane phenyl modes in complexes **1**−**3** (γ(Br) = γ(Phenylrot.)).

contrast to the experiment, where no shift was detected.[14b] This indicates that the calculations overestimate the δ_{sym}(Pyr. deformation) contribution to this mode (Discussion). The most intense band in this spectral region is located at 1006 cm^{-1} (calcd: 1018 cm^{-1}). This feature is assigned to a polarized (totally symmetric) phenyl in-plane vibration (ϕ_8). It was originally assigned to a ν(C$_\alpha$−C$_m$) vibration[14] and later reassigned to a ν(Pyr. breathing) mode.[20] However, on the basis of the calculated intensities, this band has to be assigned to the mixed phenyl δ_{sym}(C−C−C) and ν(Pyr. breathing) porphyrin vibration (calcd: 1018 cm^{-1}), which is more in agreement with ref 20. The calculated d_8 isotope shift of 1 cm^{-1} is in the correct range compared to the experimental value of 6 cm^{-1}.[14b] The observed discrepancies indicate that in this case the calculations underestimate the admixture of the porphyrin core vibration (Discussion). Finally, a weak band is found at 1030 cm^{-1} (calcd: 1054 cm^{-1}), which corresponds to an in-plane phenyl vibration (ϕ_7).

The region between 1050 and 1550 cm^{-1} contains only in-plane porphyrin core vibrations with the exception of the highly intense band at 1495 cm^{-1}, which is of the in-plane phenyl type (ϕ_5') but also has some porphyrin C−C stretching character (ν_{sym}(C$_\alpha$−C$_m$)). With the exception of the totally symmetric vibration at 1072 cm^{-1} (calcd: 1124 cm^{-1}), which is a C$_\beta$−H deformation mode (ν_9), all of the other porphyrin core vibrations are of the stretching type. The calculated frequency of ν_9 is 52 cm^{-1}, 4.9% higher in energy compared to the experimental value, which reflects the neglect of anharmonicity in the calculation (Discussion). Two totally symmetric vibrations in this region are known to be structure sensitive. The ν_{sym}(Pyr. half-ring) vibration at 1363 cm^{-1} (calcd: 1379 cm^{-1}) is both oxidation- and spin-state sensitive (band A(p) [18b]). The calculated d_8 isotope shift of 12 cm^{-1} of this mode is in excellent agreement with experiment (13 cm^{-1}).[14b] The polarized band at 1554 cm^{-1} (calcd: 1598 cm^{-1}) is assigned to a combined ν(C$_\beta$−C$_\beta$) + ν_{sym}(C$_\alpha$−C$_m$) + δ_{sym}(C$_\beta$−H) spin-state-sensitive vibration (band D(p) [18b]). The calculated d_8 isotope shift of 21 cm^{-1} is identical to the experimental value.[14b] These assignments are in agreement with the literature.[14b] One additional polarized (totally symmetric) band is found at 1233 cm^{-1} (calcd: 1260 cm^{-1}), which is assigned to ν(Pyr. breathing) + ν(C$_m$−Ph) (ν_1) with a calculated d_8 isotope shift of 3 cm^{-1}, which is again in excellent agreement with experiment (3 cm^{-1}).[14b] This assignment is partially in agreement with the literature, where this band was assigned to a pure ν(C$_m$−Ph).[20] Finally, four depolarized bands are observed in this region. Only the ν_{sym}(Pyr. half-ring) (ν_{12}) vibration at 1275 cm^{-1} (calcd: 1274 cm^{-1}) has B$_{1g}$ symmetry,[37] whereas the others at 1495, 1371, and 1467 cm^{-1} have B$_{2g}$ symmetry. Detailed assignments of these features are given in Table 3.

Finally, the two bands at the highest energy are both assigned to purely symmetric C−C stretching modes of the phenyl rings. From the polarized measurements, these have different symmetries: the band at 1597 cm^{-1} (calcd: 1650 cm^{-1}) is polarized (A$_{1g}$) and the feature at 1574 cm^{-1} (calcd 1649 cm^{-1}) is depolarized (B$_{2g}$). The larger deviations observed between the calculated and experimental frequencies for these modes (∼4%) are partly due to an intrinsic inaccuracy in the calculations (Discussion). The assignment of the band at 1597 cm^{-1} is in agreement with earlier work.[20] No d_8 isotope shift is calculated for these features. In comparison, the experimental value for the A$_{1g}$ mode is 5 cm^{-1}, [14b] indicating the presence of a small admixture of porphyrin core modes.

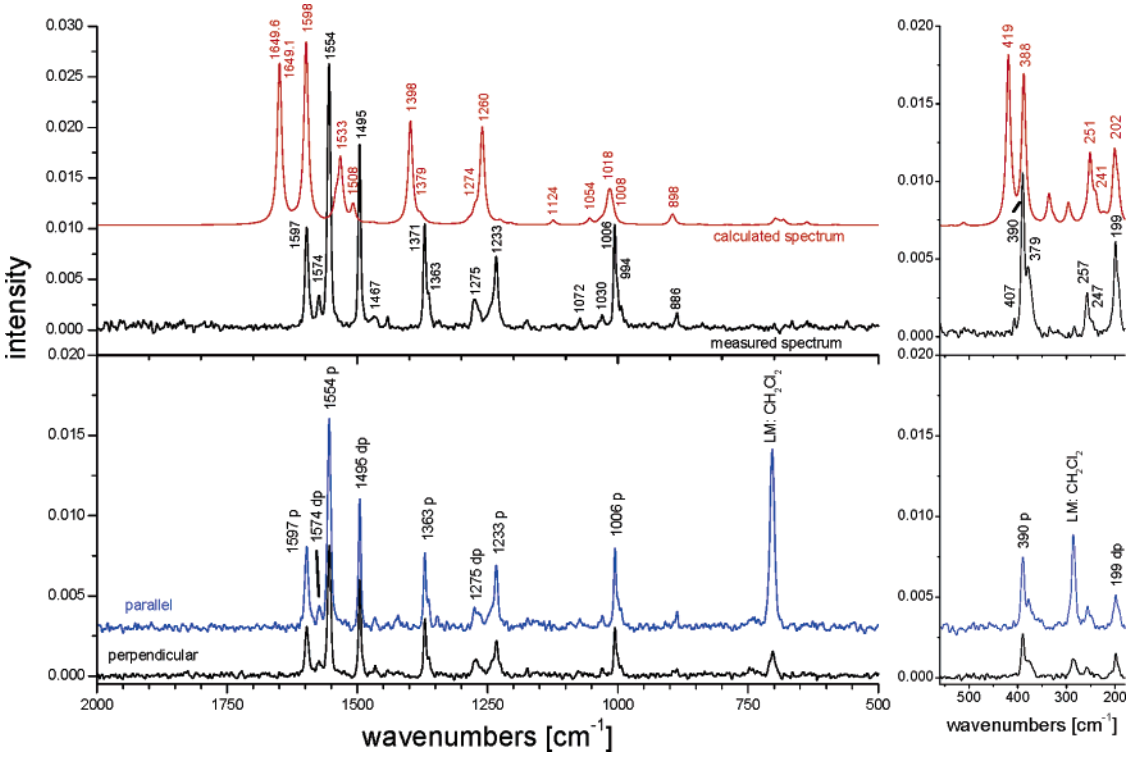

Figure 4. Comparison of the calculated and measured NR Raman spectra of **1** (top) and the polarization measurement in dichloromethane (bottom). The low energy part (560−180 cm^{-1}) of the calculated spectrum (top right) is enlarged in the Figure.

B.3. Infared Spectrum and Assignment of 1. Figure 5 shows the experimental and calculated IR spectra of **1**. As in the NR Raman case, the calculated vibrational energies are in good agreement and the IR intensities are in very good agreement with the experimental data, reproducing the overall appearance of the experimental spectrum very well. The calculated frequencies for a number of modes are too high in energy, as analyzed below. The assignments of the infrared spectrum of **1** are on the basis of the calculated energies and intensities, and the results are summarized in Table 3. In addition, calculated d_8 isotope shifts for the structure-sensitive bands I, II, and III can be compared to the experimental data[18b] reported for [Co(TPP)] and [{Fe(TPP)}$_2$O]. The IR spectrum can be divided into five regions of different types of vibrational modes.

In the far-IR region between 350 and 450 cm^{-1}, only in-plane porphyrin core vibrations are observed. The only exception is the strong band at 378 cm^{-1} (calcd: 336 cm^{-1}), which corresponds to the ν(Fe−Cl) stretching mode. More importantly, the totally symmetric Fe−N breathing vibration (ν_8) at 390 cm^{-1} (calcd: 388 cm^{-1}; vide supra) is also observed in the IR spectrum as a weak band. This is another indication of the lowered symmetry in **1** because this band is IR forbidden in D_{4h}. Two E_u symmetric vibrations are observed in this region: the feature at 402 cm^{-1} (calcd: 407 cm^{-1}) corresponds to a mixed ν(Fe−N) + δ(Pyr. translation) (ν_{50}) mode, whereas the band at 434 cm^{-1} (calcd: 444 cm^{-1}) is assigned to a Pyrrol rotation δ(Pyr. rotation) (ν_{49}). This latter feature corresponds to the spin-state sensitive band III, as defined by Oshio et al.[18b] and was identified as a low-energy porphyrin core deformation mode [18b] in agreement with our assignment. The calculated d_8 isotopic shift of 16 cm^{-1} of this feature is in excellent agreement with the observed shifts for [Co(TPP)] and [{Fe(TPP)}$_2$O] of 16 and 17 cm^{-1}.[18b]

The second region between 500 and 810 cm^{-1} mostly comprises out-of-plane vibrations. The two features at 528 (calcd: 537) and 703 cm^{-1} (calcd: 730 cm^{-1}) correspond to out-of-plane phenyl modes with E_u symmetry (π_5'' and π_4''), whereas the phenyl mode at 661 cm^{-1} (calcd: 675 cm^{-1}) is of the in-plane deformation type. Besides these highly intense bands, a very weak feature is observed at 570 cm^{-1} (calcd: 582 cm^{-1}) and assigned as shown in Table 3. The four bands between 710 and 810 cm^{-1} are all of the out-of-plane type. The intense feature at 750 cm^{-1} (calcd: 790 cm^{-1}) corresponds to a phenyl mode (π_3'') of E_u symmetry. Two out-of-plane porphyrin modes of A_{2u} symmetry are found at 720 (calcd: 750 cm^{-1}; γ_8) and 806 cm^{-1} (calcd: 847 cm^{-1}; γ_5), the latter one being the oxidation-state-sensitive band II.[18b] It was originally assigned to an in-plane deformation mode with δ(C$_\beta$−H) character,[18b] on the basis of an observed pyrrole-d_8 isotope shift. However, from the calculations, this band is associated with the intense band calculated at 847 cm^{-1} that corresponds to a γ(H$_\beta$) + γ_{sym}(Pyr. folding) vibration. This mode shows a calculated-d_8 isotope shift of 40 cm^{-1}, which is in excellent agreement with the observed shift of 35 cm^{-1} for [Co(TPP)].[18b] On the basis of these results, band II is reassigned. Finally, the very weak band at 727 cm^{-1} (calcd: 758 cm^{-1}) is assigned to an E_g vibration (γ_{20}; cf. Table 3), which gains in IR intensity via coupling with a phenyl vibration with E_u symmetry. This is another indication of the lowered symmetry in **1** because these two vibrations cannot mix in D_{4h}. The deviations in energy of about 4 to 5% between calculated and experimental

Table 3. Assignment of the Infrared (IR), NR Raman (λ_{exc} = 1064 nm), and Resonance Raman (Soret: λ_{exc} = 454.5 nm; Q_v: λ_{exc} = 514.5 nm; Q: λ_{exc} = 568.2 nm) Spectra of [Fe(TPP)(Cl)] (**1**)[a]

	mode		experimental[d] (cm^{-1})			
ν_i [h]	assignment[b]	symmetry[c]	IR	NR R[e]	RR[e]	calcd[d,f] (cm^{-1})
ϕ_4	ν_{sym}(C−C)	A_{1g}		1597 m (p)	1597 (Soret: 1598 w,p; Q_v: 1595 vw,p; Q: shoulder)	1650 s
ϕ_4''	ν_{sym}(C−C)	E_u	1597 m			1649 m
ϕ_4'	ν_{sym}(C−C)	B_{2g}		1574 w (dp)	∼1572/1577 (Soret: -; Q_v: 1571 m,dp/1576 s,dp; Q: 1573 s,dp/1578 vs,dp)	1649 m
ψ_3'	ν_3(C−C) + $\boldsymbol{\nu_{asym}(C_\alpha-C_m)}$	$A_{2u} + B_{1g}$	1574 vw			1618 vw
ν_2	$\underline{\boldsymbol{\nu(C_\beta-C_\beta)}}$ + $\boldsymbol{\nu_{sym}(C_\alpha-C_m)}$ + $\boldsymbol{\delta_{sym}(C_\beta-H)}$	A_{1g}		1554 vs (p)	∼1556 (Soret: 1557 vs,p; Q_v: 1555 s,p; Q: 1557 s,p)	1598 vs
ν_{19}	$\underline{\boldsymbol{\nu_{asym}(C_\alpha-C_m)}}$ + $\boldsymbol{\nu_{asym}(C_\alpha-C_\beta)}$ + $\boldsymbol{\delta_{asym}(C_\beta-H)}$	A_{2g}			∼1522/1516 (Soret: 1523/1517 vw; Q_v: 1523/1517 w,ap; Q: 1521/1515 m,ap)	1560
ϕ_5'	δ(C−C−H) + ν_{asym4}(C−C) + $\boldsymbol{\nu_{sym}(C_\alpha-C_m)}$	B_{2g}		1495 m (dp)	∼1495 (Soret: 1494 vw,-; Q_v: 1494 s,dp; Q: 1496 vs,dp)	1533 m
ϕ_5''	δ(C−C−H) + ν_{asym4}(C−C) + $\boldsymbol{\nu(C_\beta-C_\beta)}$ + $\boldsymbol{\nu_{asym}(C_\alpha-C_m)}$ + $\boldsymbol{\nu_{sym}(C_\alpha-C_m)}$	E_u	1486 w			1521 s
ν_{28}	$\underline{\boldsymbol{\nu_{sym}(C_\alpha-C_m)}}$ + $\boldsymbol{\nu_{asym}}$**(Pyr. half-ring)**	B_{2g}		1467 vw (dp)	1467 (Soret: -; Q_v: 1467 vw,dp; Q: 1467 vw,dp)	1508 w
ν_3	$\underline{\boldsymbol{\nu_{sym}(C_\alpha-C_m)}}$ + $\boldsymbol{\nu(C_\beta-C_\beta)}$	A_{1g}			1452 (Soret: 1452 m,p; Q_v: 1450 vw,p; Q: -)	1489
ψ_4'	ν_{asym3}(C−C) + δ(C−C−H)	A_{2u}	1440 m			1470 m
ν_{29}	$\underline{\boldsymbol{\nu}}$**(Pyr. quarter-ring)** + $\boldsymbol{\nu(C_m-Ph)}$	B_{2g}		1371 m (dp)	∼1371 (Soret: -; Q_v: 1370 s,dp; Q: 1372 m,dp)	1398 m
ν_4	$\underline{\boldsymbol{\nu_{sym}}}$**(Pyr. half-ring)**	A_{1g}		1363 w	∼1363 (Soret: 1364 s,p; Q_v: 1361 m,p; Q: 1365 m,p)	1379 vw
ν_{20}	$\underline{\boldsymbol{\nu}}$**(Pyr. quarter-ring)** + $\boldsymbol{\delta_{sym}(C_\beta-H)}$ + δ(C−C−H) + ν_2(C−C)	A_{2g}			∼1335 (Soret: -; Q_v: 1334 m,ap; Q: 1336 m,ap)	1373
ν_{41}	$\boldsymbol{\delta_{asym}(C_\beta-H)}$ + $\boldsymbol{\nu(C_m-Ph)}$ + $\underline{\boldsymbol{\nu_{sym}}}$**(Pyr. half-ring)** $\boldsymbol{\nu_{asym}(C_\alpha-C_\beta)}$	E_u	1340 m 1334 m			1369 s
ν_{12}	$\underline{\boldsymbol{\nu_{sym}}}$**(Pyr. half-ring)**	B_{1g}		1275 w (dp)	1278 (Soret: 1278 vw,-; Q_v: 1278 w,dp; Q: 1278 m,dp)	1274 vw
ν_{27}	$\boldsymbol{\nu}$**(Pyr. quarter-ring)** + $\underline{\boldsymbol{\nu(C_m-Ph)}}$ + ν_1(C−C)	B_{2g}			∼1266 (Soret: 1266 vw,dp; Q_v: 1265 w,dp; Q: 1266 m,dp)	1286 vvw
ν_1	$\boldsymbol{\nu}$**(Pyr. breathing)** + $\underline{\boldsymbol{\nu(C_m-Ph)}}$	A_{1g}		1233 m (p)	∼1233 (Soret: 1235 m,p; Q_v: 1230 w,p; Q: 1232 w,p)	1260 m
ν_{26}	$\underline{\boldsymbol{\delta_{asym}(C_\beta-H)}}$ + $\boldsymbol{\nu_{sym}}$**(Pyr. quarter-ring)**	A_{2g}			∼1225 (Soret: -; Q_v: 1225 w,ap; Q: 1226 vw,ap)	1248
ν_{36}	$\boldsymbol{\nu_{sym}}$**(Pyr. half-ring)** + $\boldsymbol{\nu}$**(Pyr. quarter-ring)** + $\underline{\boldsymbol{\nu(C_m-Ph)}}$	E_u	1200 w			1250 w
ν_{34}	$\underline{\boldsymbol{\delta_{asym}(C_\beta-H)}}$ + $\boldsymbol{\nu_{asym}(C_\alpha-C_\beta)}$	B_{2g}			1182 (Soret: -; Q_v: 1181 w,dp; Q: 1182 w,dp)	1226

Table 3 (Continued)

	mode		experimental[d] (cm^{-1})			
ν_i [h]	assignment[b]	symmetry[c]	IR	NR R[e]	RR[e]	calcd[d,f] (cm^{-1})
ν_{51}	**ν(Pyr. quarter-ring) + ν(Pyr. breathing)**	E_u	1175 m			1236 m
ϕ_6''	δ_{sym}(C−C−H)	E_u	1158 w			1223 w
ν_{17}	**δ_{sym}(C$_\beta$−H)**	B_{1g}			1080 (Soret: -; Q_v: 1081 w,dp; Q: 1080 m,dp)	1125
ν_9	**δ_{sym}(C$_\beta$−H)**	A_{1g}		1072 vw	~1072 (Soret: 1073 m,p; Q_v: 1070 m,p; Q: 1073 m,p)	1124 vw
ψ_8'	ν_{asym1}(C−C) + δ(C−C−H)	A_{2u}	1070 m			1106 m
ν_{52}	**δ_{sym}(C$_\beta$−H)**	E_u				1117 w
ϕ_7	ν_1(C−C)	A_{1g}		1030 vw	~1029 (Soret: -; Q_v: 1028 vw,p; Q: 1030 vw,p)	1054 w
ν_{30}	**ν_{asym}(Pyr. half-ring)**	B_{2g}			~1017 (Soret: -; Q_v:1015 w,dp; Q:1018 s,dp)	1035
ν_{15}	**ν(Pyr. breathing)**	B_{1g}				1030
ϕ_8	δ_{sym}(C−C−C) + **ν(Pyr. breathing)**	A_{1g}		1006 m (p)	1006 (Soret: 1006 w,p; Q_v: 1006 w,p; Q: 1006 m,p)	1018 w
ϕ_8''	δ_{sym}(C−C−C) + **ν(Pyr. breathing) + ν_{asym}(Pyr. half-ring)**	E_u	1002 vs			1017 s
ν_{47}	**ν(Pyr. breathing) + δ_{asym}(Pyr. deformation)** + $\nu_{breathing}$(C−C)	E_u	995 vs			1005 s
ν_6	**ν(Pyr. breathing)** + $\nu_{breathing}$(C−C)	A_{1g}		994 vw (p)	994 (Soret: -; Q_v: 993 w,p; Q: 994 m,p)	1008 w
ν_7	**δ_{sym}(Pyr. deformation)** + γ_2(H)	A_{1g}		886 vw (p)	887 (Soret: 887 w,p; Q_v: 887 vw,p; Q: 887 vw,p)	898 w
ν_{32}	**δ_{asym}(Pyr. deformation)**	B_{2g}			851 (Soret: -; Q_v: 850 vw,dp; Q: 851 w,dp)	890
ν_{16}	**δ_{sym}(Pyr. deformation)** + γ_1(H)	B_{1g}				874
γ_5	**γ(H$_\beta$) + γ_{sym}(Pyr. folding)**	A_{2u}	806 s			847 s
core	overtone 390 cm^{-1}	A_{1g}			779 (Soret: -; Q_v: 779 m,p; Q: 778 vw,p)	
π_3''	γ_1(H)	E_u	750 s			790 vs
π_3	γ_1(H)	B_{1g}			744 (Soret: -; Q_v: -; Q: 744 w,dp)	781
		A_{1g}			723 (Soret: 723 vw,p; Q_v: 723 vw,p; Q: -)	
γ_{20}	**γ_{sym}(Pyr. folding) + γ_{asym}(Pyr. folding) + γ(H$_\beta$)** + γ_1(H)	$E_g + E_u$	727 vw			758
γ_8	**γ_{sym}(Pyr. folding) + γ(H$_\beta$)** + γ_1(H)	A_{2u}	720 m			750
π_4''	γ_2(C)	E_u	703 s			730 s
ϕ_9''	δ_2(C−C−C) + **δ(Pyr. rotation)**	E_u	661 m			675 m
ϕ_9	δ_2(C−C−C)	A_{1g}			639 (Soret: 639 vw,p; Q_v: -; Q: -)	652
	combination band (184 + 391 cm^{-1})	A_{1g}			572 (Soret: 572 vw,p; Q_v: 570 w,p; Q: -)	
γ_7	**γ(C$_\alpha$−C$_m$) + γ_{asym}(Pyr. folding) + γ_{sym}(Pyr. folding)**	A_{2u}	570 vw			582 vw

Table 3 (Continued)

	mode		experimental[d] (cm^{-1})			
ν_i [h]	assignment[b]	symmetry[c]	IR	NR R[e]	RR[e]	calcd[d,f] (cm^{-1})
π_5''	γ_1(C) + **δ(Pyr. translation)**	E_u	528 m			537 m
ν_{49}	**δ(Pyr. rotation)**	E_u	434 s			444 m
σ_{13}''	τ(ring twist)	E_g		407 vw	408 (Soret: -; Q_v: -; Q: 408 vw,-)	419 w
ν_{50}	**ν(Fe−N)** + **δ(Pyr. translation)**	E_u	402 m			407 m
ν_8	**$\nu_{breathing}$(Fe−N)**	A_{1g}	390 m	390 m (p)	391 (Soret: 392 s,p; Q_v: 390 vs,p; Q: 390 w,p)	388 w
Fe−Cl	**ν(Fe−Cl)**		378 s	379 w		336
		A_{1g}			257 (Soret: 258 vw,p; Q_v: 257 w,p; Q: 258 vw,p)	
γ_{16}	**γ(Pyr. tilting)** + γ(Phenylrot.)[g]	$B_{2u} + B_{1g}$		257 vw	258 (Soret: -; Q_v: -; Q: -; $\lambda_{exc.}$= 647.1 nm: 258 vw,dp)	251 vw
Ph	γ(Phenylrot.)[g] + **γ(Pyr. tilting)**	$B_{1g} + A_{2u}$		247 vw	247 (Soret: -; Q_v: -; Q: 247 vw, dp; 647.1 nm: 247 vw,dp)	241 vw
	porphyrin breathing				203 (Soret: 204 vw,p; Q_v: 202 w,p; Q: 202 vw,p)	200 vw
ν_{18}	**ν(Fe−N)**	B_{1g}		199 w (dp)	199 (Soret: -; Q_v: -; Q: -; 647.1 nm: 199 vw,dp)	202 vw

[a] For notations of in-plane and out-of-plane core modes see Li et al.[10a,10c] and Figures S6 and S7. [b] Assignment in local coordinates: see Table 2 and Figure 3 for the phenyl coordinates and ref 10a and c (Figures S6 and S7) for the in-plane and out-of-plane porphyrin coordinates. Porphyrin coordinates are printed in bold. Assignments for [Ni(TPP)] by Rush III et al.[13] are underlined. [c] Effective D_{4h} symmetry: see the Results and Analysis section. [d] Calculated (DFT) and experimental intensity (vs = very strong, s = strong, m = middle, w = weak, and vw = very weak). [e] Depolarization ratio: p = polarized, dp = depolarized and ap = anomalous polarized band. [f] Calculated with B3LYP/LanL2DZ: see Experimental section. [g] γ(Phenylrot.) corresponds to $\nu(Ph)_1$ = γ(Br) in bromobenzene. [h] Labeling used by Spiro and co-workers (cf. ref 13).

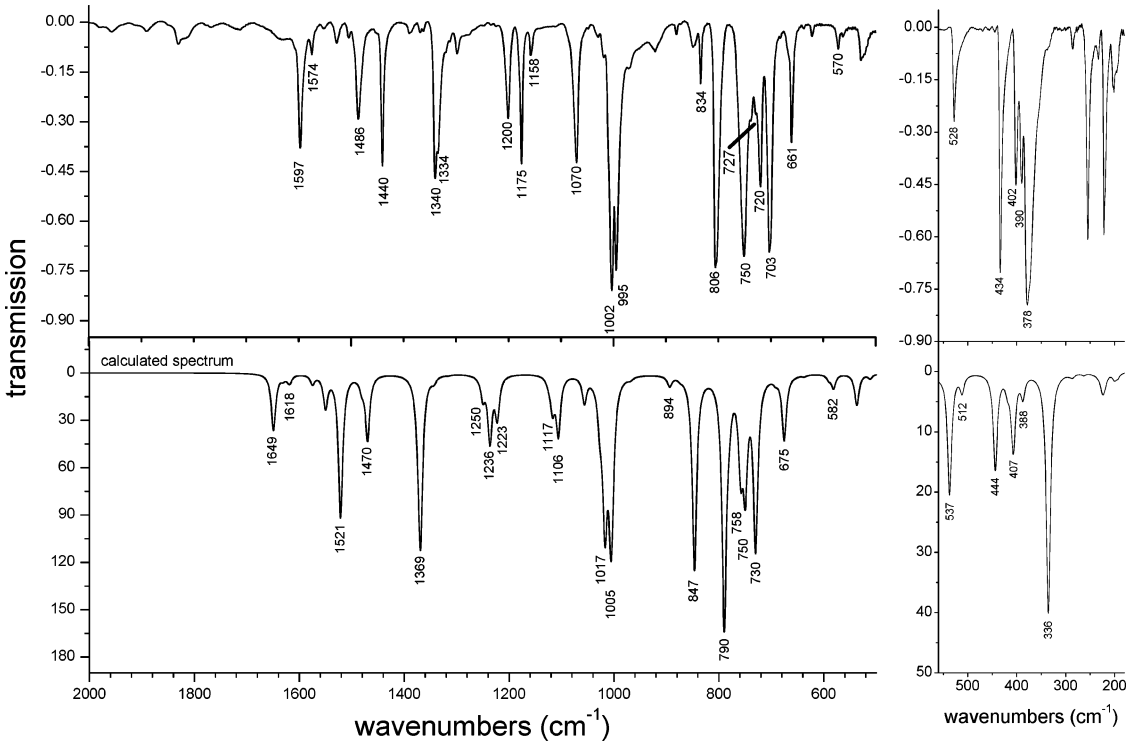

Figure 5. IR spectrum of **1**: the measured spectrum (top) and the calculated spectrum (bottom).

frequencies observed for the phenyl C−H deformation (π_4'', π_3 and π_3'') and the $\gamma(H_\beta)$ porphyrin vibrations in this region are due to the neglect of anharmonicity in the calculations (cf. Discussion).

The third region between 990 and 1160 cm^{-1} mostly comprises in-plane vibrations. The strong band at 995 cm^{-1} (calcd: 1005 cm^{-1}) is assigned to a ν(Pyr. breathing) + δ_{asym}(Pyr. deformation) porphyrin core vibration with $\nu_{breathing}$(C−C) phenyl contribution (ν_{47}), whereas the intense feature at 1002 cm^{-1} (calc.: 1017 cm^{-1}) corresponds to the mixed δ_{sym}(C−C−C) + ν(Pyr. breathing) + ν_{asym}(Pyr. half-ring) mode with mostly phenyl character (ϕ_8''). Both have E_u symmetry. The assignment of the strong band at 1070 cm^{-1} is not entirely clear. One possibility is a $\delta_{sym}(C_\beta-H)$ core mode with E_u symmetry, which is calculated at 1117 cm^{-1} (ν_{52}). Alternatively, this feature could be identified as the ν_{asym1}(C−C) + δ(C−C−H) phenyl vibration (ψ_8') with A_{2u} symmetry, calculated at 1106 cm^{-1}. A d_8 isotope substitution would be necessary to distinguish between these possibilities. Finally, the band at 1158 cm^{-1} is assigned to a phenyl vibration as shown in Table 3.

The following region between 1160 and 1350 cm^{-1} mostly consists of E_u symmetric in-plane porphyrin vibrations. The two bands at 1175 (calcd: 1236 cm^{-1}) and 1200 cm^{-1} (calcd: 1250 cm^{-1}) are both in-plane porphyrin stretching modes, which show deviations in energy of 4 to 5% between calculation and experiment (cf. Discussion) and are assigned as shown in Table 3. The band at 1340 cm^{-1} (calcd: 1369 cm^{-1}) is assigned to a mixed $\delta_{asym}(C_\beta-H)$ + $\nu(C_m-Ph)$ + ν_{sym}(Pyr. half-ring) + $\nu_{asym}(C_\alpha-C_\beta)$ vibration and is known to be spin-state-sensitive (band I [18b]). It appears split into two components in **1**, where a shoulder at 1334 cm^{-1} is present. Previously, this band was assigned to a $\nu(C_\alpha-C_m)$ + $\nu(C_m-Ph)$ by Oshio et al.[18b] The calculated d_8 isotope shift for this band of 19 cm^{-1} shows some deviation from the experimental value (8 cm^{-1}) obtained for [Co(TPP)].[18b] However, this is most probably due to the highly mixed nature of this mode, where, depending on the actual complex, changes in the contributions of individual local coordinates can be expected to occur.

The region at the highest energy between 1400 and 1600 cm^{-1} consists only of phenyl-type vibrations, which are assigned as shown in Table 3. For ϕ_4'', the frequency is obtained 52 cm^{-1} higher in energy compared to experiment. The reason for this is discussed in section B.2 for the corresponding modes ϕ_4 and ϕ_4', which are combinations of the same local coordinate but with different symmetries (cf. Table 3). The weak band at 1574 cm^{-1} (calcd: 1618 cm^{-1}) corresponds to the ν_3(C−C) phenyl vibration of A_{2u} symmetry, which is mixed with the IR forbidden $\nu_{asym}(C_\alpha-C_m)$ porphyrin vibration with B_{1g} symmetry. Hence, this is another indication of the symmetry lowering in **1**. The band at 1486 cm^{-1} (calcd: 1521 cm^{-1}) is assigned to a strongly mixed in-plane vibration (ϕ_5'') of the δ(C−C−H) + ν_{asym4}(C−C) phenyl and $\nu(C_\beta-C_\beta)$ + $\nu_{asym}(C_\alpha-C_m)$ + $\nu_{sym}(C_\alpha-C_m)$ porphyrin type. From the calculations, we have classified this band as a phenyl type mode, but the individual contributions might vary experimentally depending on the actual complex investigated.

B.4. Resonance Raman Spectra of 1 and Assignment. The electronic spectra of metalloporphyrins have been explained on the basis of the four-orbital model of Gouterman.[38] They are dominated by the two $\pi \rightarrow \pi^*$ transitions from the a_{1u} and a_{2u} HOMOs to the e_g LUMO of the porphyrin dianion. Both resulting excited states have E_u symmetry and show a strong configuration interaction (CI). This leads to two well-separated bands in the absorption spectra, the intense Soret band (where the individual transition moments are additive), and the weak Q band (where they nearly cancel). In addition, a third band is observed on the higher energy side of Q. This band, Q_v, is a result of vibronic mixing between the Soret and the Q band. Because both excited states are of E_u symmetry, vibronic mixing is enabled by the vibrations of A_{2g}, B_{1g}, and B_{2g} symmetries.[39] For the resonance Raman spectra of metalloporphyrins, A-, B-, and C-term enhancement mechanisms are important.[40] A-term enhancement is caused by a displacement of the excited state relative to the ground state and is in general only relevant for totally symmetric modes. Because A-term intensity is proportional to the square of the electric dipole transition moment of the excited electronic state, this mechanism is dominant in the region of the Soret transition. B-term enhancement is caused by the vibronic coupling between the excited state $|e\rangle$ and another excited state $|s\rangle$, which leads to the resonance enhancement of the vibrations that are effective in coupling these states. Hence, this mechanism applies to the Q band, where vibrations of A_{2g}, B_{1g}, and B_{2g} symmetries are enhanced. Additional A-term enhancement of A_{1g} modes in the Q region is also expected. Thus, resonance enhancement of nontotally symmetric modes is therefore indicative of the presence of vibronic bands in the absorption spectra. However, B_{1g} and B_{2g} enhancements could theoretically also be induced by a Jahn−Teller distortion of the excited states with E_u symmetry.[41] Hence, *the enhancement of A_{2g} modes is the most diagnostic for the presence of vibronic coupling.* A_{2g} modes are easily identified in the Raman spectra because of their anomalous polarization (ap; $\rho > 3/4$), which relates to the scattering tensor being antisymmetric.[42−44] Finally, C-term enhancement is observed upon the excitation to a vibronic sideband of a forbidden or weakly allowed 0−0 electronic transition[40] that leads to the enhancement of overtones and combination modes. This applies to the Q_v region of the absorption spectra. These different types of resonance enhancement are indeed observed for complex **1**, as shown in Figure S2. Figures 8−10 present the RR spectra of **1** including the polarized data in Q (λ_{exc} = 568.2 nm), Q_v (λ_{exc} = 514.5 nm), and Soret (λ_{exc} = 454.5 nm) resonance. Figure 7 shows the absorption spectrum of **1** indicating the different excitation wavelengths. The RR data in the Soret region are dominated by polarized (A_{1g}) bands, which can therefore easily be identified from the Soret spectrum. The Q and Q_v spectra of **1** contain depolarized, polarized, and anomalous polarized bands. The presence of A_{2g} vibrations in the Q and Q_v spectra confirms well the presence of vibronic coupling as already discussed. The Q_v RR spectra also show overtones and

(43) Placzek, G. In *Handbuch der Radiologie;* Marx, E., Ed.; Akademische Verlagsgesellschaft: Leipzig, Germany, 1934; Vol. 6, Part 2, p 205.
(44) Spiro, T. G.; Strekas, T. C. *Proc. Natl. Acad. Sci. U.S.A.* **1972**, *69*, 2622−2626.

combination bands above 1600 cm^{-1} corresponding to C-term enhancement, which confirms that Q_v is the vibronic sideband of Q.

A number of new bands are observed in the RR spectra compared to the NR Raman spectra. The assignments of the RR data included in Table 3 are on the basis of the energies of the bands in correlation to the DFT results as well as the symmetries determined from the polarized experiments. In some cases, calculated d_8 isotope shifts for **1** in comparison to experimental shifts obtained for [Ni(TPP)][13] are used to further confirm the assignments. The ν(Fe−N) breathing mode at 390 cm^{-1} is strongly enhanced in the Q_v region of compound **1**, which is surprising because this band has A_{1g} symmetry; therefore, one would anticipate its maximum enhancement in the Soret region (Figure S3).[45] The band at 639 cm^{-1} (calcd: 652 cm^{-1}) in Soret resonance is assigned to an in-plane δ_2(C−C−C) phenyl vibration (ϕ_9) with A_{1g} symmetry. This feature shows no d_8 isotope shift in the calculations and is in agreement with results for [Ni(TPP)].[13] The depolarized band at 744 cm^{-1} (calcd: 781 cm^{-1}) observed in Q resonance corresponds to an out-of-plane γ_1(H) phenyl vibration (π_3) with B_{1g} symmetry. The calculated d_8 isotope shift of 10 cm^{-1} for this mode is in good agreement with the value of 7 cm^{-1} observed for [Ni(TPP)].[13] Two new depolarized bands are observed at 851 and 1017 cm^{-1} in Q and Q_v resonances, respectively. In both cases, two possible features with B_{1g} and B_{2g} symmetries are present in the calculations as well as in the RR spectra of [Ni(TPP)]. Hence, no assignments of these bands are possible. The depolarized band at 1080 cm^{-1} observed in Q and Q_v resonances is assigned as shown in Table 3. The depolarized band observed at 1182 cm^{-1} in Q_v and Q resonances corresponds to either the calculated vibration at 1226 cm^{-1} (a $\delta_{asym}(C_\beta-H) + \nu_{asym}(C_\alpha-C_\beta)$ core mode) or the feature predicted at 1222 cm^{-1} (a phenyl vibration); both have B_{2g} symmetry. In [Ni(TPP)],[13] a band at 1190 cm^{-1} with a small phenyl-d_{20} shift is observed and assigned to the $\delta(C_\beta-H)$ vibration calculated at 1226 cm^{-1}. Because a larger d_{20} isotope shift is expected for the phenyl vibration, the band at 1182 cm^{-1} is tentatively assigned to this feature. The modes at 744 cm^{-1} (phenyl vibration), ν_{17}, and ν_{34} (both $C_\beta-H$ in-plane porphyrin vibrations) show larger deviations in energy between calculation and experiment compared to those of the other porphyrin modes, which are due to the neglect of anharmonicity (Discussion). The weak, anomalous polarized bands at 1225 and 1335 cm^{-1} in Q and Q_v resonances are assigned as shown in Table 3. The depolarized band at 1266 cm^{-1} (calcd: 1286 cm^{-1}) is observed in all RR spectra. It is assigned to a mixed ν(Pyr. quarter-ring) + $\nu(C_m-Ph)$ porphyrin core vibration with phenyl contribution (ν_1(C−C)) with B_{2g} symmetry (ν_{27}). The calculated d_8 isotope shift of 2 cm^{-1} is in very good agreement with experiment (1 cm^{-1} for [Ni(TPP)][13]). The band at 1452 cm^{-1} in Soret and Q_v resonances is assigned to the mixed in-plane $\nu_{sym}(C_\alpha-C_m) + \nu(C_\beta-C_\beta)$ porphyrin vibration (ν_3) with A_{1g} symmetry. The split, anomalous polarized band [46] at 1522/1516 cm^{-1} (calcd: 1560 cm^{-1}) is assigned to the mixed $\nu_{asym}(C_\alpha-C_m) + \nu_{asym}(C_\alpha-C_\beta) + \delta_{asym}(C_\beta-H)$ in-plane porphyrin core vibration and is known to be spin-state sensitive (band C(ap)[47,18b]). It was originally assigned to only $\nu(C_\alpha-C_m)$.[14b] The predicted d_8 isotope shift of this feature is 6 cm^{-1}. All of these assignments are listed in Table 3.

B.5. Effects of Symmetry Lowering. There are three major effects resulting from the symmetry lowering from idealized D_{4h} to the actual symmetry of [Fe(TPP)(Cl)]. Because of the fact that the phenyl rings are no longer perpendicular to the porphyrin core, the coupling between the core and the phenyl vibrations becomes stronger. The second effect is that modes with different symmetries in D_{4h} appear mixed in **1**. Several examples are observed in the NR Raman and IR spectra as discussed above, where even (g) and odd (u) vibrations are combined. This applies, for example, to the NR Raman bands at 247 and 257 cm^{-1} and the IR bands at 390, 727, and 1574 cm^{-1}. Of importance though is the fact that all of these symmetry-breaking modes obtain only very small intensities because of this intensity-stealing mechanism. This together with the observation of polarized, depolarized, and anomalous polarized bands clearly shows that the $[Fe(TPP)]^+$ core of **1** still behaves as if it has D_{4h} symmetry. The third effect of symmetry lowering beyond C_{4v} in **1** is that degenerate E_u vibrations appear to be split in the IR spectra. However, the observed splittings are very small (about 5 cm^{-1}). Hence, this again indicates that an effective D_{4h} symmetry is present in **1**.

C. Vibrational Spectra and Assignments of Compounds 2 and 3 in Comparison with Those of 1. The crystal as well as the DFT optimized structures of complexes **1**−**3** are very similar overall, as discussed in section A. Correspondingly, the averaged metal−nitrogen distances are similar and increase in the order of Co (1.985 Å) < Mn (2.019 Å) < Fe (2.049 Å). The most pronounced difference among **1**, **2**, and **3** occurs for the metal−chloride bond distances, which increase in the order of Co (2.145 Å) < Fe (2.192 Å) ≪ Mn (2.389 Å). Another important difference is observed for the out-of-plane displacement of the metal atom from the N_4 plane of the porphyrin, which increases in the order of Co (0.05 Å) < Mn (0.258 Å) < Fe (0.383 Å). On the basis of the large structural similarities of complexes **1**−**3**, it can be expected that the overall vibrational properties of the corresponding $[M(TPP)]^+$ units are quite similar. The only exception is the metal−chloride stretching vibration, where larger differences should be observed.

Figure 6 shows the NR Raman data of **2** together with the calculated spectrum. In this case, exceptional agreement is obtained between theory and experiment. The corresponding spectra of **3** are presented in Figure S1. The agreement between the calculated and experimental data is also very good in this case. As already discussed for **1**, small shifts of certain bands to higher energy (average deviation in energy of about 2 to 3%) are also observed in the calculations for

(45) The excitation profile is a plot of the Raman intensity versus the Raman excitation energy.

(46) The origin of the splitting is not known. It might relate to the fact that the spectrum was recorded in a KBr disk.

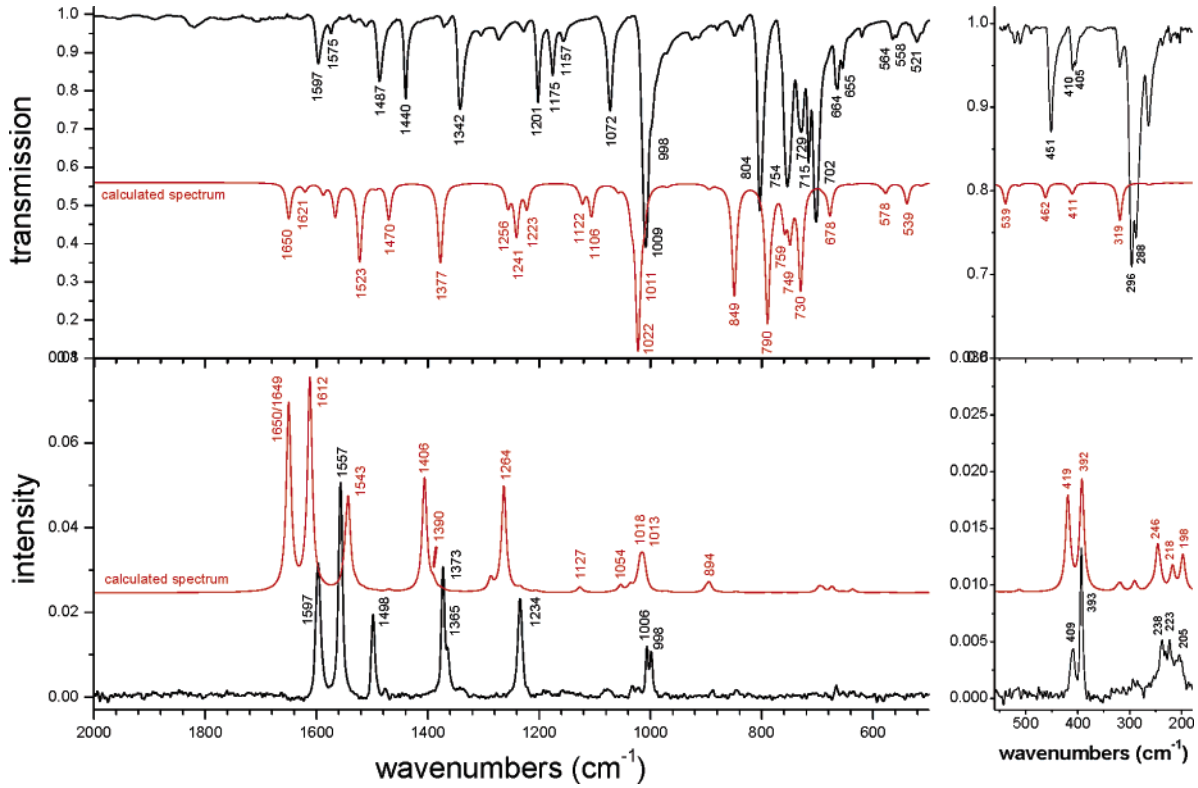

Figure 6. IR spectrum of **2** (top) and the NR Raman spectrum of **2** (bottom). The corresponding calculated spectra are included in the two panels as indicated. The low energy part (560−180 cm^{-1}) of the calculated spectra is enlarged.

Table 4. Comparison of Metal−Chloride Stretching Frequencies (cm^{-1}) and QCC-NCA as well as Calculated (DFT) Force Constants *f*(M−Cl) (mdyn/Å) for [M(TPP)Cl] (**1**, **2**, and **3**) and Model Systems [M(P*)Cl] (**1̃a**, **2̃a**, and **3̃a**)

	ν(M−Cl)				ν(M−Cl)	*f*(M−Cl)	
compound	calcd[b,f]	exptl[c]	lit.	model	PED[a,f]	calcd[b]	QCC-NCA
1	263/*336*	378	360[2] 364[57] [d]	**1̃a**	225 (9%)/*339* (86%)	1.419	1.796
2	263/*319*	296	299[57] [e]	**2̃a**	235 (39%)/*318* (74%)	1.160	0.932
3	286/*398*	397		**3̃a**	262 (40%)/*396* (82%)	1.704	1.717

[a] PED = potential energy distribution; the numbers in parentheses correspond to the % contribution of the M−Cl coordinate to this mode. [b] Calculated with B3LYP/LanL2DZ; see Experimental section. [c] Experimental infrared frequencies. [d] Determined from Raman data of [Fe(OEP)(Cl)]. [e] Determined from Raman data. [f] The ν(M−Cl) vibration is mixed with a porphyrin mode, and hence there are two vibrations that carry ν(M−Cl) contributions. As shown in the PED, the mode at higher energy has more M−Cl stretching character.

2 and **3** (Discussion). Because of the structural similarities of **1**−**3**, it is not surprising that the NR Raman spectra of these compounds show large similarities as evidenced by a comparison of Figures 4, 6, and S1. Hence, the assignments of the NR Raman spectra of **2** and **3** listed in Tables S1 and S2, respectively, largely parallel the assignments for **1**. Only a few differences are observed. The band at 1574 cm^{-1} in the experimental NR Raman spectrum of **1** is not observed in the spectra of compounds **2** and **3**. This band corresponds to the phenyl in-plane vibration ν_{sym}(C−C) (ϕ_4') with B_{2g} symmetry. However, complex **3** shows an additional small band at 1540 cm^{-1} that could not be unambiguously assigned. The metal−chloride stretching vibration only appears in the NR Raman spectrum of **1**. Otherwise, the same vibrations are observed in the NR Raman spectra of **1**−**3**. Some of them show small characteristic shifts, which are discussed in section E.

Figure 6 shows the IR data of **2** together with the calculated spectrum. Again, in this case, the most exceptional agreement is obtained between theory and experiment. The corresponding spectra of **3** are presented in Figure S1. A good agreement between theory and experiment is also achieved in this case. The IR spectra of all three compounds **1**−**3** basically show the same normal modes. Correspondingly, the appearances of the MIR spectra are very similar. However, the far-IR spectra look clearly different because the metal−chloride and the metal−nitrogen stretching vibrations are located in this region, which show the strongest metal sensitivity (cf. section E).

D. Metal−Chloride Bonding. For compounds **1** and **3**, the experimental frequency of the metal−chloride stretching vibration is similar with ν(Fe−Cl) = 378 cm^{-1} and ν(Co−Cl) = 397 cm^{-1} (cf. Table 4). In contrast, the Mn−Cl stretching vibration of 296 cm^{-1} is located at a significantly lower energy. This trend is in agreement with the metal−chloride distances with **3** (2.145 Å) < **1** (2.192 Å) ≪ **2** (2.389 Å). As mentioned in section A, the metal−chloride bond lengths are overestimated in the calculations, especially for compound **1**. Correspondingly, the calculated frequency obtained for **1** of 336 cm^{-1} is significantly lower than the

experimental value, whereas for **2** (319 cm^{-1}) and **3** (398 cm^{-1}) a very good agreement is observed. To compare the M−Cl bond strengths in these compounds rigorously, accurate M−Cl force constants are necessary and require a normal coordinate analysis (NCA). For this purpose, simple model systems [Fe(P)(Cl)] ($\tilde{\mathbf{1}}$), [Mn(P)(Cl)] ($\tilde{\mathbf{2}}$), and [Co(P)(Cl)] ($\tilde{\mathbf{3}}$; P = porphine) were fully optimized, and the force constants were calculated as listed in Table 4. In the next step, a mass of 77 was used for the meso hydrogens of these models corresponding to the phenyl groups. This leads to models $\tilde{\mathbf{1}}$**a**, $\tilde{\mathbf{2}}$**a**, and $\tilde{\mathbf{3}}$**a**, which accurately reproduce the M−Cl frequencies of full model systems **1**−**3** applying TPP (cf. Table 4). This is an important result because it shows that the simple porphine ligand is a good approximation for TPP when only the properties of the central M−Cl unit are considered. Finally, using the QCC-NCA procedure,[21] the M−Cl force constants were fitted to reproduce the experimental M−Cl stretching frequencies. In this way, experimental force constants for compounds **1**, **2**, and **3** of 1.796, 0.932, and 1.717 mdyn/Å, respectively, were obtained. The NCA force constants show that the Fe−Cl and Co−Cl bonds are twice as strong as the Mn−Cl bond. The reason for this rather surprising result is evidenced by an analysis of the MO diagrams of these complexes. For this purpose, models $\tilde{\mathbf{1}}$−$\tilde{\mathbf{3}}$ were used because porphine has proven to be a good model for TPP, considering the presence of the M−Cl bond. The coordinate system is chosen such that the *z* axis is aligned with the M−Cl bond, whereas the *x* and *y* axes are oriented along the M−N bonds of the porphyrin ligand. Hence, the $d_{x^2-y^2}$ orbital of the metal undergoes a strong σ bond with the pyrrole nitrogens of the porphyrin, whereas d_{xy} is partially nonbonding. However, the metal−chloride σ bond is mediated by the orbital d_{z^2}, whereas d_{xz} and d_{yz} are potentially involved in π bonds with the chloride ligand. Note that the principal bonding scheme of [Fe(TPP)(Cl)] has been analyzed before; however, the main focus was the metal−porphyrin interaction.[48]

[Co(TPP)(Cl)] (**3**) has the simplest electronic structure due to the low-spin d^6 configuration of Co(III) ($S = 0$), which corresponds to a $[d_{xy},d_{xz},d_{yz}]^6 \equiv [t_2]^6$ configuration of the metal. Hence, the unoccupied d_{z^2} orbital undergoes a strong σ bond with the filled p_z orbital of the chloro ligand, where the corresponding bonding combination has 29% d_{z^2} and 58% chloro p_z character. Because the d_{xz} and d_{yz} orbitals of the metal are fully occupied, no π bond with the p_x and p_y orbitals of chloride is possible. In summary, the metal−Cl bond in **3** can be described as a strong (pure) σ bond. In comparison, compound **1** is a high-spin d^5 complex with $S = {}^5/_2$ ground state. In the spin-unrestricted scheme, this means that all α-d orbitals are fully occupied and hence, do not contribute to the bonding with σ- or π-donor ligands. Therefore, all metal−ligand bonding comprises unoccupied β-d orbitals. The Fe−Cl σ bond is mediated by the interaction of d_{z^2} and p_z of the chloro ligand. The corresponding bonding combination has 26% iron d_{z^2} and 60% chloro p_z orbital contributions, which corresponds to a strong σ bond. Additional π bonds between the d_{xz} and d_{yz} orbitals of iron and the p_x and p_y orbitals of the chloro ligand, respectively, are also present. The corresponding bonding combinations have about 10% metal and about 45% chloride character indicative of a medium-strength interaction. Therefore, complex **1** formally has one-half of a σ bond and one π bond. Compared to **3**, the σ bond is reduced by 50%, whereas an additional π bond is present. These effects seem to cancel, giving almost identical M−Cl force constants in these complexes.

Compound **2** is a high-spin d^4 complex with $S = 2$ ground state and a $[d_{xz},d_{yz},d_{xy},d_{z^2}]^4$ electron configuration. Compared to complex **1**, the α-$d_{x^2-y^2}$ orbital is unoccupied and therefore, similar M−Cl interactions would be expected in **1** and **2**. However, the force constants show that this is not the case. The Mn−Cl σ bond between d_{z^2} and the p_z orbital of chloride is somewhat weaker compared to that in **1** as evidenced by the 16% metal d_{z^2} and 57% chloro p_z character of the corresponding bonding combination. The largest difference occurs for the M−Cl π bond. The corresponding bonding combinations between d_{xz} and d_{yz} of Mn(III) and p_x and p_y of chloride only have about 2% metal and 75% chloro character, respectively, which corresponds to a very weak interaction. Therefore, the M−Cl bond in complex **2** corresponds only to half a σ bond. This is the reason for the much smaller M−Cl force constant of only 0.932 mdyn/Å in **2** compared to 1.796 mdyn/Å for **1**.

E. Metal-Sensitive Bands in the Raman and IR Spectra of 1−3. Boucher and Katz[49] measured the IR spectra of several divalent metal complexes of protoporphyrin IX and hematoporphyrin IX dimethyl ester and identified three metal-sensitive bands at 920−980, 500−525, and 350−365 cm^{-1}, but no definitive assignments could be made. The skeletal stretching and breathing modes were found to only have small shifts within the experimental uncertainty. Nakamoto and co-workers assigned the metal−nitrogen stretching bands of a series of OEP and TPP complexes on an empirical basis.[50,18a] The observed shifts were attributed to the variable occupation of the σ-antibonding $d_{x^2-y^2}$ orbital in these complexes. Hence, vibrations that contain a direct contribution of the M−N stretching coordinate should be the most affected. However, the oxidation- and spin-state sensitive IR bands I−III and Raman bands A, C, D, and E (band B is characteristic for penta coordination) as described in the Introduction should also be sensitive to the metal ion.[18] The frequency shifts of bands I and III were correlated to the metal−porphyrinato nitrogen distances[18b] in agreement with Nakamoto's analysis.

In the IR and NR Raman spectra of **1**, 50 and 36% of the observed modes, respectively, are of the phenyl type, which show no shifts or show only small frequency shifts.[51] In contrast, frequency shifts are observed for most porphyrin

(47) Chottard, G.; Battioni, P.; Battioni, J.-P.; Lange, M.; Mansuy, D. *Inorg. Chem.* **1981**, *20*, 1718−1722.
(48) Cheng, R.-J.; Chen, P.-Y.; Lovell, T.; Liu, T.; Noodleman, L.; Case, D. A. *J. Am. Chem. Soc.* **2003**, *125*, 6774−6783.
(49) Boucher, L. J.; Katz, J. J. *J. Am. Chem. Soc.* **1967**, *89*, 1340−1345.
(50) Ogoshi, H.; Masai, N.; Yoshida, Z.; Takemoto, J.; Nakamoto, K. *Bull. Chem. Soc. Jpn.* **1971**, *44*, 49.
(51) Very small shifts of some of these bands that were observed can be traced back to small admixtures of porphyrin core vibrations.

Table 5. Metal-Sensitive Bands (Also Oxidation- and Spin-State-Sensitive) in the Infrared, NR Raman, and RR Spectra of **1**−**3**[a]

		FeTPPCl (**1**)		MnTPPCl (**2**)		CoTPPCl (**3**)	
		experimental	calcd[b]	experimental	calcd[b]	experimental	calcd[b]
	M−N (Å), averaged	2.049	2.09	2.019	1.99	1.985	1.99
IR[18b]	band I, spin (cm^{-1})	1340/1334	1369	1342	1377	1351	1387
	band II, ox. (cm^{-1})	806	847	804	849	795	848
	band III, spin (cm^{-1})	434	444	451	462	465	475
R[18b]	band A, ox., and spin (cm^{-1})	1363	1379	1365	1390	1359	1393
	band B[c] (cm^{-1})	1371	1398	1373	1406	1372	1408
	band C, spin (cm^{-1})	1522/1516	1560	1538/1532	1588		1588
	band D, spin (cm^{-1})	1554	1598	1557	1612	1563	1626
	band E, ox. (cm^{-1})	390	388	393	392	403	390
IR	ν(M−Cl)	378	336	296	319	397	399
	ν_{50} (cm^{-1})	402	407	410/405	411	?	411
R	ν_{18} (cm^{-1})	199	202	223	218	255 ?	238

[a] Frequencies are given in cm^{-1}. [b] Calculated with B3LYP/LanL2DZ. [c] Band B is a marker band for five-coordinate porphyrin complexes.[47,18b]

Table 6. Selected Crystallographic Distances (Å) for Compound **1** (cf. Ref 28), **2** (This Article), and **3** (cf. Ref 33) that are Important for the Structure-Sensitive Bands[a]

compound	d(M−N)	d(C_m−Ph)	d(C_β−C_β)	d(C_α−C_β)	d(C_α-N)	d(M−Ct)	d(C_α−C_m)
[Fe(TPP)(Cl)] (**1**)	2.04(9)	1.50(8)	1.38(0)	1.44(6)	1.38(4)	0.383	1.39(9)
[Mn(TPP)(Cl)] (**2**)	2.019	1.496	1.357	1.440	1.385	0.258	1.399
[Co(TPP)(Cl)] (**3**)	1.985	1.518	1.360	1.446	1.372	0.05	1.391

[a] Distances are averaged over chemically equivalent bonds.

core vibrations in the [M(TPP)(Cl)] complexes, but only a few of them are of considerable size as already correctly stated by Boucher and Katz. The bands with large shifts are mostly vibrations with a large M−N stretching contribution as proposed before.[18,50] Hence, frequency shifts are mostly expected for bands below 500 cm^{-1}. Table 5 lists the experimental and calculated frequencies of the eight spin- and oxidation-state-sensitive bands known from the literature for complexes **1**−**3**. In the IR spectra, the three porphyrin vibrations I−III show metal sensitivity. In the NR Raman spectra, three modes show significant shifts for complexes **1**−**3** (band A, D, and E). Hence, only six of the eight structurally sensitive bands from the literature are metal-sensitive in the [M(TPP)(Cl)] series studied here. Three additional metal sensitive bands are identified here. These are ν_{18} (from NR Raman), ν_{50} (IR), and the M−Cl stretching vibration as discussed in section D (cf. Table 4). Corresponding to the relatively small frequency shifts observed for **1**−**3** as shown in Table 5, the underlying differences in complex geometries must be small. Therefore, to analyze the reasons for the appearance of the shifts, detailed assignments of the corresponding vibrations as obtained in this study are necessary. For the stretching vibrations, the differences in the vibrational frequencies can be correlated with the differences in bond lengths. However, the interpretation of the metal sensitivity of the deformation modes is not straightforward.

Vibrations with a considerable M−N contribution are observed in the low-energy region of the spectra. The metal−nitrogen distances decrease in the order of Fe (2.049 Å) > Mn (2.019 Å) > Co (1.985 Å), and hence the frequencies of vibrations with ν(M−N) character are expected to increase in the order of Fe < Mn < Co. There are three vibrations with a pure or mostly M−N stretching contribution observed in complexes **1**−**3**. The most intense band corresponds to the totally symmetric $\nu_{breathing}$(M−N) vibration (band E, ν_8), which increases in the order of 390 cm^{-1} (Fe) < 393 cm^{-1} (Mn) < 403 cm^{-1} (Co) in agreement with this trend. The ν(M−N) vibrations with B_{1g} symmetry (ν_{18}) observed in the NR Raman spectra of **1**−**3** also strongly follows this trend as shown in Table 5. Finally, the ν(M−N) vibrations with E_u symmetry (ν_{50}) observed in the IR spectra of **1** and **2** are mixed with the δ(Pyr. translation) porphyrin deformation mode. Nevertheless, the correlation also applies here where this feature appears at 402 cm^{-1} in **1** and at 410/405 cm^{-1} in **2**. The fact that this band is split in **2** reflects a small degree of symmetry lowering from ideal D_{4h} symmetry (cf. section B.5).

Bands A, C, and D in the Raman and band I in the IR spectra of **1**−**3** correspond to in-plane porphyrin stretching vibrations (cf. Table 3); therefore, their frequencies can be correlated with C−C, C−N, and M−N distances as observed in the crystal structures of **1**−**3** (cf. Table 6). Band A corresponds to the in-plane ν_{sym}(Pyr. half-ring) porphyrin vibration. Hence, the frequency of this mode relates to changes in the metal−nitrogen, the C_α−C_β and the C_α−N distances. However, because the observed frequency shifts are very small, a quantitative interpretation of the observed behavior of this mode is not possible. For band C, the observed frequency is larger for the Mn than for the Fe complex. This mode has considerable ν_{asym}(C_α−C_m) character; however, the C_α−C_m distance is comparable in the two complexes, as shown in Table 6. However, this mode also has some C_α−C_β contribution, and the corresponding C_α−C_β distance is slightly larger for **1** compared to that for **2**, which is consistent with the observed trend in frequencies (cf. Table 5). The totally symmetric metal-sensitive band D, which is assigned to a ν(C_β−C_β) + ν_{sym}(C_α−C_m) porphyrin vibration with a small amount of δ_{asym}(C_β−H) contribution, is observed in both the NR Raman and RR spectra of **1**−**3**.

The frequency of this mode increases in the order of **1** < **2** < **3**, as shown in Table 5. This can be traced back to differences in the C−C bond lengths of the porphyrin core. First, the $C_\beta-C_\beta$ distances are almost identical for **2** and **3**, whereas they are elongated in **1**. However, complexes **1** and **2** have almost identical $C_\alpha-C_m$ distances, whereas this bond is shorter in complex **3**. These trends are consistent, leading to the observed frequency shifts of this band. Finally, band I corresponds to the mixed $\delta_{asym}(C_\beta-H) + \nu(C_m-Ph) + \nu_{sym}$(Pyr. half-ring) $+ \nu_{asym}(C_\alpha-C_\beta)$ in-plane porphyrin vibration. The frequency shift of this band cannot be analyzed because of a large number of different contributions. For example, the C_m-Ph distances behave inversely to the M−N distances. Besides these stretching vibrations, two deformation modes (bands II and III; cf. Table 5) are also found to be metal-sensitive. Band II corresponds to the out-of-plane $\gamma(H_\beta) + \gamma_{sym}$(Pyr. folding) porphyrin deformation mode and hence, the frequency shift of this vibration is difficult to interpret. The energy increases in the order of Co ≪ Mn < Fe. The frequency shift of band III, which is an in-plane δ(Pyr. rotation) porphyrin deformation mode, seems to be correlated to the out-of-plane displacement of the metal, which increases in the order of Co < Mn < Fe. Correspondingly, the observed trend in the vibrational energies is Co > Mn > Fe.

Discussion

In this study, the vibrational properties of the five-coordinate porphyrin complexes [M(TPP)(Cl)] (M = Fe, Mn, and Co) are analyzed in detail. For complex [Fe(TPP)(Cl)] (**1**), nonresonance Raman (NR Raman) spectra including polarized data are presented for the first time. Resonance Raman (RR) spectra of this compound are also reported, including Soret, Q, and Q_v resonance data together with polarized measurements. In addition, MIR and FIR spectra of **1** are presented. Hence, a complete vibrational data set for complex **1** is obtained in this study. These data are then assigned in detail using calculated vibrational energies as well as calculated NR Raman and IR intensities, which show very good agreement with experiment overall (vide infra). Additional information that assists in assigning the spectra is available from (a) the polarized measurements that allow for the determination of the symmetries of the different vibrations and (b) d_8 isotope data reported in the literature for a number of complexes.[13,14b,18b] The assignments are based on an idealized model system [M(TPP)] with D_{4h} symmetry. For the phenyl mode assignment, local internal coordinates derived from bromobenzene are used. On the basis of all this information, a complete and consistent assignment of all of the spectroscopic data obtained for **1** has been achieved. So far, no detailed vibrational assignments for five-coordinate porphyrin complexes such as [Fe(TPP)(Cl)] are available from the literature, where most of the research has been focused on four-coordinate complexes. For compound **1**, only a small number of totally symmetric modes from the Soret RR spectrum (λ_{exc} = 457.9 nm) have been assigned before,[20] on the basis of a simple comparison of the obtained spectra with those of [Ni(TPP)]. Additional bands in the Raman and IR spectra of **1** were identified and classified, but no further analysis was performed.[14,18b] The assignments obtained in this study are in general consistent with recent work by Rush III et al., who assigned the RR and IR spectra of [Ni(TPP)] based on a DFT-SQM analysis.[13] In some cases, large deviations in vibrational frequencies (for example, ν_2 is located at 1554 cm^{-1} in **1** and at 1572 cm^{-1} in [Ni(TPP)]) are observed. In addition, because of very good agreement between the calculated and experimental NR Raman and IR spectra obtained here, more sophisticated assignments of the observed vibrations were possible in this study, as indicated in Table 3. The complete analysis of the vibrational spectra of **1** performed here also leads to the reassignment of a number of bands. These include features at 1233, 1006, and 886 cm^{-1} in the Raman spectra of **1** (cf. Table 3). The prominent band at 390 cm^{-1}, which is one of the structure-sensitive bands identified by Burke et al.,[14b] is reassigned to the totally symmetric $\nu_{breathing}$(Fe−N) vibration on the basis of the calculated NR Raman spectra and the excellent agreement between its calculated and experimental pyrrole-d_8 isotope shift. This is in agreement with the assignments for [Ni(TPP)].[10a,13] The IR spectra of complex **1** are assigned here for the first time with the exception of structure-sensitive bands I−III. However, band II at 806 cm^{-1} is reassigned in this work to the out-of-plane $\gamma(H_\beta) + \gamma_{sym}$(Pyr. folding) porphyrin core vibration on the basis of the calculated IR spectra and the excellent agreement between its calculated and experimental pyrrole-d_8 isotope shift. In addition, a number of new bands are assigned in this study. These include the important bands at 402 cm^{-1} in the IR (ν_{50}) and 199 cm^{-1} in the Raman spectrum (ν_{18}) of **1**, which correspond to the Fe−N stretching vibrations with E_u and B_{1g} symmetries. These modes have not been assigned yet. Similar to the corresponding A_{1g} mode at 390 cm^{-1}, these are also strongly metal-sensitive and probably oxidation- and spin-state-sensitive.

A general shift of the vibrational frequencies of **1**−**3** to somewhat higher energy (average deviation: about 2 to 3%) is observed in the calculations compared to experiment. However, in some cases, larger deviations (up to 5%) are observed. These can be traced back to different effects depending on the nature of the respective modes. First, large shifts (about 5%) are observed for the three combinations of the ν_{sym}(C−C) stretching mode of the phenyl rings (ϕ_4, ϕ_4', ϕ_4'' in Table 3), which occur just below 1600 cm^{-1}. In this case, the deviations are partly due to an intrinsic inaccuracy of the B3LYP/LanL2DZ method. This is evident from frequency calculations on benzene. As shown in Table S7, ν_{sym}(C−C) is calculated at 1641 and observed at 1594 cm^{-1} (average), which corresponds to a deviation of 2.9%. Interestingly, using the much more time consuming B3LYP/TZVP method does not lead to an improvement for this mode. The second class of vibrations in which larger deviations of the frequencies are observed correspond to in-plane and out-of-plane C−H deformation modes. This especially includes the $\delta(C_\beta-H)$ and $\gamma(H_\beta)$ core vibrations and the δ(C−C−H) bends of the phenyl rings. (See, for example, $\delta(C_\beta-H)$ at about 1100 cm^{-1}, $\gamma(H_\beta)$ at about 800

cm^{-1}, and δ(C−C−H) at about 1100 cm^{-1}, as listed in Table 3.) These deviations are due to the neglect of anharmonicity effects in the theoretical treatment. Calculations on benzene show that C−H vibrations usually show significant degrees of anharmonicity (cf. Table S7). These calculations indicate that ν_{sym}(C−C) is also affected by deviations due to anharmonicity. Finally, differences are observed for the amount of mixing between phenyl and porphyrin core vibrations, which applies to a small number of modes (Results and Analysis). This is evident from a comparison of calculated and experimental d_8 isotope shifts, which reflect the porphyrin core mode contribution. In the case of **1**, the calculated structure shows smaller dihedral angles between the phenyl substituents and the porphyrin core compared to the crystal structure. Hence, this rotation of the phenyl rings toward the porphyrin plane introduces changes in mode mixing of phenyl and porphyrin core vibrations. This most probably explains the observed deviations.

Three major effects of symmetry lowering from the idealized D_{4h} symmetry of the $[M(TPP)]^+$ core are observed for complexes **1**−**3**. Compared to four-coordinate [Ni(TPP)] and corresponding systems, the chloro complexes studied here show the additional complexity of having open shells, a larger distortion of the porphyrin core, and axial ligands. From vibrational spectra, these deviations from D_{4h} are manifested in (i) enhanced coupling between porphyrin core and phenyl vibrations, (ii) the combination of even (g) and odd (u) vibrations, and (iii) small splittings of the degenerate E_u vibrations. However, these effects are very small and therefore, together with the observation of polarized, depolarized, and anomalous polarized bands in the Raman spectra, this clearly shows that the $[M(TPP)]^+$ cores of **1**−**3** still behave as if they have D_{4h} symmetry. As discussed above, the assignments of the vibrational spectra of complexes **1**−**3** are therefore carried out in an effective D_{4h} symmetry. The overall vibrational properties of the $[M(TPP)]^+$ units in complexes **1**−**3** are quite similar, which relates to the large structural similarities of the metalloporphyrin cores of these systems. The largest differences are observed in the low-energy region of the spectra, where the M−Cl and the M−N stretching vibrations are observed. On the basis of our analysis, it is possible to give more precise assignments of the metal-sensitive modes than before, as inferred by Oshio et al.[18b] in 1984: "In order to understand the structure-sensitivity of these bands on a quantitative basis, it is necessary to carry out theoretical calculations [...]." Not surprisingly, it is found that modes with mostly phenyl character do not show noticeable shifts. In the case of porphyrin core vibrations, frequency shifts are in general observed for most vibrations; however, only a few of them are of considerable size. Of the eight oxidation and spin-state-sensitive bands known from the literature,[18] five are found to be metal-sensitive in the [M(TPP)(Cl)] series studied here. These are bands A, D, and E (RR) and bands I−III (IR). In addition, two more metal-sensitive porphyrin core vibrations are identified here (ν_{50} and ν_{18}, vide supra). Bands with large M−N stretching contributions are sensitive because of the differences in the M−N bond lengths in **1**−**3**,

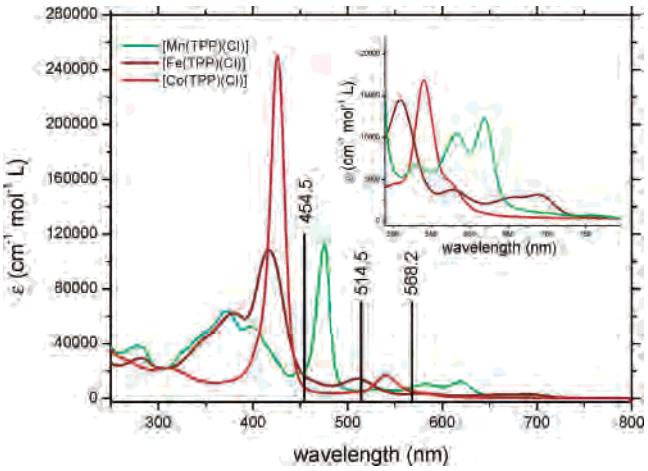

Figure 7. Solution absorption spectra of compound **1** (brown) measured in chloroform, of compound **2** (green) in a 1/1 mixture of butyronitrile and propionitrile, and of compound **3** (red) in methanol. The spectra are scaled with absorption coefficients taken from the literature.[58,59,33]

Table 7. Absorption Bands Observed in the UV−Vis Absorption Spectra of Complexes **1**−**3** (in nm)

[Fe(TPP)Cl] (**1**)		[Mn(TPP)(Cl)] (**2**)		[Co(TPP)(Cl)] (**3**)	
position	assignment	position	assignment	position	assignment
379	Cl → M CT	390	Soret		
417	Soret	476	P → M CT	426	Soret
510	Q_v	530	?	540	Q_v
578	?	583	Q_v	574	Q
654	P → M CT	620	Q		
690	P → M CT ?				

Scheme 2

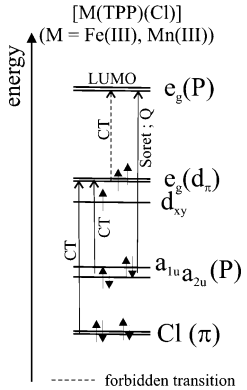

which applies to bands E, ν_{50}, and ν_{18}. These occur in the low-energy region of the spectra. Bands I, A, C, and D correspond to porphyrin core stretching modes. In this Article, we have developed a model where the shifts of these bands are interpreted on the basis of differences in the porphyrin C−C and C−N and the metal−N distances. The interpretation of the frequency shifts of remaining vibrations I and II is not straightforward because of the fact that these are deformation modes.

Besides the analysis of the metal-sensitive modes, we have investigated the strength of the metal−chloride interaction in complexes **1**−**3**. To this end, the M−Cl stretching vibrations have been assigned, and from normal coordinate analysis (NCA), M−Cl force constants of 1.796 (Fe−Cl), 0.932 (Mn−Cl), and 1.717 mdyn/Å (Co−Cl) have been determined. These large differences in M−Cl bond strengths

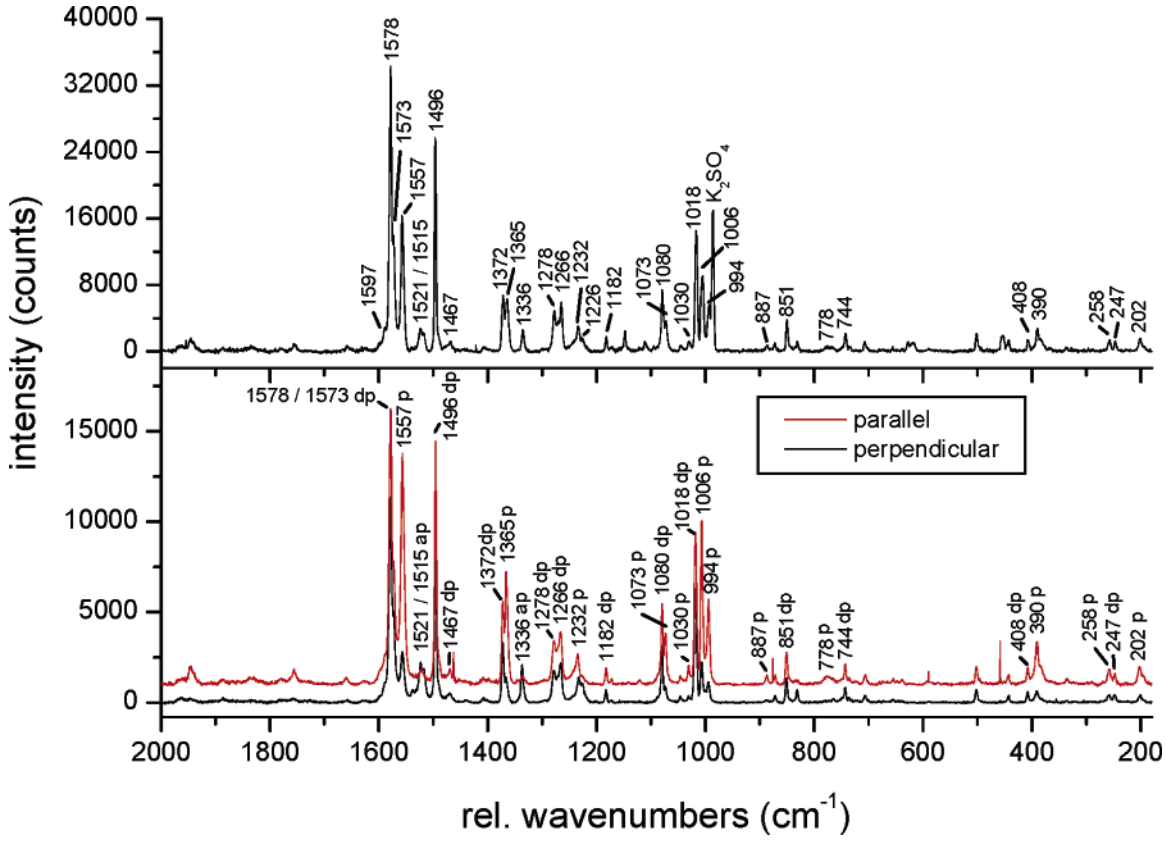

Figure 8. Resonance Raman spectra of **1**, excited at 568.2 nm (Q resonance). The RR spectra were measured with potassium sulfate as the internal standard (top). The polarized measurement is shown on the bottom.

are reflected by the M−Cl bond distances of 2.192 Å in **1**, 2.389 Å in **2** and 2.145 Å in **3**. For **2**, this value is obtained from a new crystal structure presented here. An analysis of the MO diagrams of **1**−**3** allows for a determination of the electronic structural reasons for these differences. In the case of compound **1**, the Fe−Cl bond can roughly be classified as one-half of a σ bond and one π bond. In comparison, the Co−Cl bond in **3** corresponds to one σ bond. The similar M−Cl force constants obtained for **1** and **3** indicate that the enhanced σ and the reduced π interaction in **3** compared to those in **1** seem to compensate and lead to comparable bond strengths. The strongly reduced M−Cl bond strength in **2** compared to that in **1** (and **3**) is mostly due to a lack of the M−Cl π bond in this complex. Correspondingly, the Mn−Cl bond only corresponds to half a σ bond in agreement with the observed reduction of the force constant by half in **2** (0.932 mdyn/Å) compared to that in **1** (1.796 mdyn/Å).

Besides its use for the determination of vibrational energies, RR spectroscopy offers detailed insight into the nature of electronically excited states. This relates to the mechanism of resonance enhancement and the actual nature of enhanced vibrations. For metalloporphyrins, A-, B- and C-term enhancements are important,[40] as described in section B.4. The A-term mechanism is dominant in the region of the intense Soret transition and leads to the enhancement of totally symmetric modes. B-term enhancement is found in the region of Q and Q_v bands and relates to vibronic coupling, which is manifested in the enhancement of anomalous polarized A_{2g} modes. Complex **3** shows the simplest absorption spectrum of compounds **1**−**3**, investigated here (cf. Figure 7). In this case, the Soret transition is located at 426 nm (cf. Table 7). At lower energy, the band at 540 nm is assigned to Q_v and the shoulder at 574 nm to the Q band, which is in agreement with the assignments for [Co(TPP)] from the literature.[38] These assignments are further confirmed using RR spectroscopy. Excitation at 514.5 and 568.2 nm leads to the enhancement of the anomalous polarized vibration ν_{20} at 1335 cm^{-1} (cf. Table S2). This indicates that the band at 540 nm is the Q_v band and the shoulder at about 574 nm must then correspond to Q. The separation of these features of about 1100 cm^{-1} supports this assignment.[38] The fact that no other bands are observed in the absorption spectrum of **3** relates to the low-spin d^6 electron configuration of the metal, which prohibits low-energy porphyrin → metal or chloride → metal charge-transfer transitions.

The absorption spectrum of compound **1** is more complicated and shows at least six bands at 379, 417, 510, 578, 654, and 690 nm (cf. Table 7). Because of the high-spin d^5 configuration of iron in this complex, porphyrin to metal charge-transfer (P → M CT) transitions can now occur (cf. Scheme 2). These $a_{1u}(\pi)$, $a_{2u}(\pi) \rightarrow e_g(d_\pi)$ CT transitions have been assigned to bands near 600 nm for high-spin Fe^{III} porphyrin complexes.[15a] Because the corresponding excited states have E_u symmetry in idealized D_{4h} symmetry, strong CI mixing with the nearby Q excited state might also occur. In addition, chloro to iron charge-transfer transitions (Cl → M CT) might also be present in the spectra. The Soret band in complex **1** appears split with its components located at

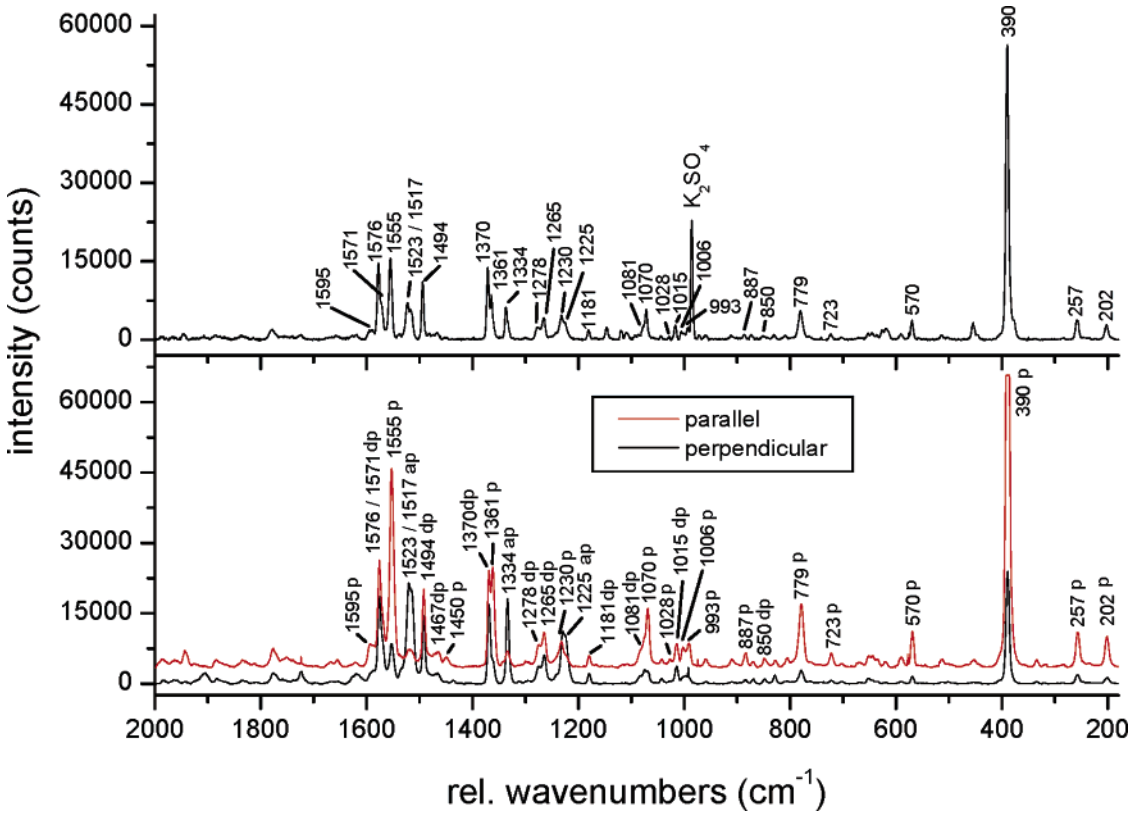

Figure 9. Resonance Raman spectra of **1**, excited at 514.5 nm (Q_v resonance). The RR spectra were measured with potassium sulfate as the internal standard (top). The polarized measurement is shown on the bottom. In the perpendicular measurement, the 390 cm^{-1} band is cut off because of its large intensity.

about 379 and 417 nm (cf. Figure 7). Further insight into these band assignments can be gained from RR measurements. The RR spectrum of **1**, excited at 454.5 nm shows mostly totally symmetric vibrations (cf. Figure 10); therefore, the absorption band at 417 nm is assigned to the Soret band. From the literature, the 379 nm band has been assigned to a chloride → Fe^{III} charge-transfer transition.[52,53] However, the large intensity of this band indicates that the corresponding excited state might steal some intensity from the Soret band. The remaining four absorption bands are located in the Q region of **1**. The RR spectrum of **1**, excited at 568.2 nm (cf. Figure 8) shows a weak band, and the data obtained at 514.5 nm (cf. Figure 9) show medium-intensity anomalous polarized bands, indicating vibronic coupling (anomalous polarized bands that are typically observed are located at about 1520 and 1335 cm^{-1}). In addition, overtones are enhanced with excitation into the absorption band at 510 nm (cf. Figure S2), which indicates that this band is actually the Q_v band (see Section B.4). Hence, a possible assignment might be that Q and Q_v correspond to the bands at about 578 and 510 nm, respectively. However, the separation of these absorption bands of about 2350 cm^{-1} is too large. It should only be about 1250 cm^{-1}, as determined by Gouterman.[38] Hence, the Q band is probably weak in **1** and masked by the feature at 578 nm, the nature of which is not known. The RR spectrum, excited at 647.1 nm (cf. Figure S5), shows not only the usually observed porphyrin A_{2g} modes at 1335 and 1522 cm^{-1} but also the low-energy anomalous polarized bands (Figure S5) that are not observed at any other excitation wavelength. These low-energy bands correspond to in-plane porphyrin deformation modes with some phenyl out-of-plane mode contribution. Hence, the band at 654 nm shows a completely different excitation behavior than the usual Q and Q_v band enhancements. This indicates that the band at 654 nm might correspond to the P → Fe CT transition in agreement with the prediction from the literature.[1] Because this transition leads to two excited states with E_u symmetries (cf. Scheme 2), the second component could correspond to the band at 690 nm, but this is only speculative.

In the case of **2**, the absorption spectrum shows two strong bands in the Soret region at 476 (band V[54]) and 390 nm (band VI)[55] (cf. Table 7). This has been attributed to a CI mixing of the Soret excited state with the porphyrin to metal $a_{1u}(\pi)$, $a_{2u}(\pi)$ → $e_g(d_\pi)$ charge-transfer states with E_u symmetry[38] (cf. Scheme 2). Note that this requires a shift of the P → M CT states from the visible to the UV region compared to that in **1**. Because of the stronger RR enhancement of low-energy vibrations observed, including Mn−X (X = halide) and Mn−N stretching modes in the region of band V in [Mn(ETP)(Cl)] (ETP = etioporphyrin I), this feature

(52) Spiro, T. G.; Li, X.-Y. In *Resonance Raman Spectra of Heme and Metalloproteins;* Spiro, T. G., Ed.; Wiley: New York, 1988; pp 1−37.
(53) Hendrickson, D. N.; Kinnaird, M. G.; Suslick, K. S. *J. Am. Chem. Soc.* **1987**, *109*, 1243−1244.
(54) Boucher, L. J. *Coord. Chem. Rev.* **1972**, *7*, 289−329.
(55) Parthasarathi, N.; Hansen, C.; Yamaguchi, S.; Spiro, T. G. *J. Am. Chem. Soc.* **1987**, *109*, 3865−3871. (b) Gaughan, R. R.; Shriver, D. F.; Boucher, L. J. *Proc. Natl. Acad. Sci. U.S.A.* **1975**, *72*, 433.

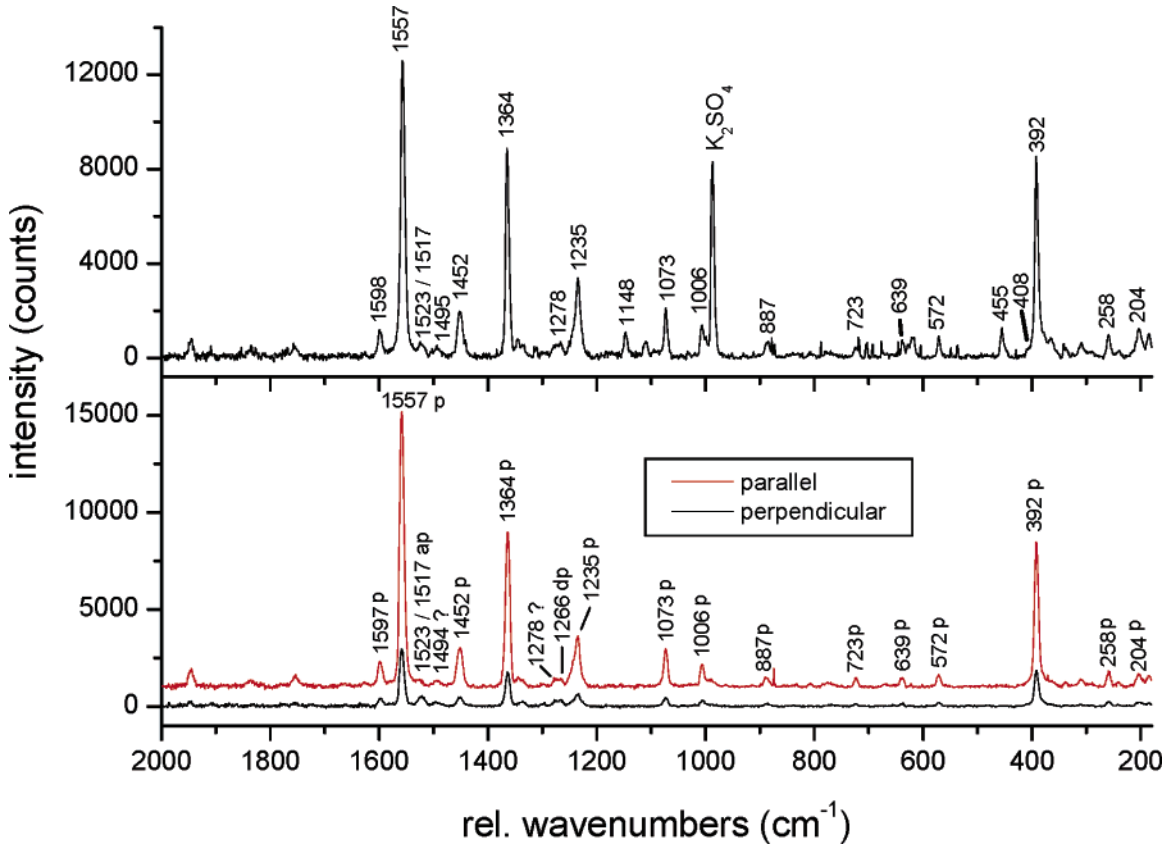

Figure 10. Resonance Raman spectra of **1**, excited at 454.5 nm (Soret resonance). The RR spectra were measured with potassium sulfate as the internal standard (top). The polarized measurement is shown on the bottom.

has been assigned to the predominant CT transition.[56] Note that Soret excitation in general leads to the enhancement of higher-energy porphyrin core vibrations. A stronger enhancement of the low-energy bands in the RR spectrum upon excitation at 488 nm is also found for compound **2** compared to that in the Soret RR spectra of **1** and **3**, indicating that this analysis is correct. It is important to note that the most intense band in this spectrum for **2** is the feature at 393 cm^{-1}, which corresponds to the totally symmetric $\nu_{breathing}$(Mn−N) vibration. The RR excitation profiles of this mode differ significantly for compounds **2** and **1**, as shown in Figures S3 and S4. For complex **1**, the maximum enhancement appears in Q_v resonance, whereas complex **2** shows the maximum upon excitation into band V. More importantly, the RR spectrum of **2**, excited at 454.5 nm shows anomalous polarized bands indicating the vibronic character of band VI, which is centered around 390 nm. This has also been observed by Parthasarathi et al.,[55] who obtained two anomalous polarized bands at 1339 and 1529 cm^{-1} upon excitation at 406.7 nm in **2**. This indicates that the simple hyperporphyrin model by Gouterman[38] might not be sufficient to explain the occurrence of bands V and VI in [Mn(TPP)(Cl)]. In the lower-energy region, the RR spectrum obtained at an excitation wavelength of 568 nm again shows anomalous polarized bands that indicate vibronic coupling. Therefore, the band at about 583 nm is assigned to the vibronic band, Q_v, and the band at 620 nm to Q (cf. Table 7). The separation of these bands of about 1020 cm^{-1} is in agreement with this assignment. In addition, corresponding bands at 560 and 592 nm in [Mn(ETP)(Cl)] have also been attributed to these features.[56] Finally, the nature of the band at about 530 nm is not clear. Anomalous polarized bands are present in the RR spectra but only with low intensity upon excitation at 514.5 nm.

Acknowledgment. We gratefully acknowledge the financial support provided by the Deutsche Forschungsgemeinschaft (DFG; grant LE 1393/1). F.P. acknowledges the Fonds der Chemischen Industrie (FCI) for a Chemiefonds-fellowship. We acknowledge Mrs. U. Cornelissen for recording the Raman spectra of compounds **1**−**3**.

Supporting Information Available: IR and Raman spectra of **3**, RR spectra of **1**, excitation profiles of $\nu_{breathing}$(M−N) for **1** and **2**, and illustrations of the local coordinates used for the classification of in- and out-of-plane porphyrin core modes by Li et al. Assignments of the vibrational data of complexes **2** and **3**, and details of the crystal structure determination of **2**, including atomic coordinates, anisotropic displacement parameters, and geometric parameters. Coordinates of the DFT fully optimized structures of **1**−**3** are also included. This material is available free of charge via the Internet at http://pubs.acs.org.

IC0510866

(56) Asher, S.; Sauer, K. *J. Chem. Phys.* **1976**, *64*, 4115−4125.
(57) Kitagawa, T.; Abe, M.; Kyogoku, Y.; Ogoshi, H.; Watanabe, E.; Yoshida, Z. *J. Phys. Chem.* **1976**, *80*, 1181−1186.
(58) Browett, W. R.; Fucaloro, A. F.; Morgan, T. V.; Stephens, P. J. *J. Am. Chem. Soc.* **1983**, *105*, 1868−1872.
(59) Mu, X. H.; Schultz, F. A. *Inorg. Chem.* **1992**, *31*, 3351−3357.